



Université  
Paris Cité



Politecnico  
di Torino

# Université Paris Cité - Politecnico di Torino

Double degree program in:  
Quantum Devices and Nanotechnologies for ICTs

Academic Year 2021/2022  
July 2022

## Optically coupled optomechanical crystals: toward Chaos and Collective dynamics

Beltramo Gregorio

Under supervision of Rémy Braive



université  
PARIS-SACLAY

The Master thesis has been carried out at Centre de Nanosciences et de Nanotechnologies, C2N, a joint research unit, between CNRS (Centre National de la Recherche Scientifique) and Université Paris-Saclay, devoted to Photonics, Fundamental Physics, Material Science and Quantum technologies located in Palaiseau, Île-de-France, France.

More precisely, I have been working for four months in the ToniQ group, belonging to the Department of Photonics, that is in charge of Non-linear Nanophotonics and Quantum Information study. The group is composed by: Rémy BRAIVE, Robert HORVATH (Post-doc), Gladys JARA-SCHULZ (PhD) and Théo MARTEL (PhD).

The master thesis period has been about Non-linear Nanophotonics addressed by Photonic Crystal Optomechanics.

# Contents

<b>1</b>	<b>Introduction to opto-mechanics</b>	<b>3</b>
1.1	Optical resonator . . . . .	3
1.2	Mechanical resonator . . . . .	4
1.3	Opto-mechanical coupling . . . . .	5
1.4	Readout mechanism of mechanical oscillations . . . . .	5
1.5	Overview of optomechanical devices in literature . . . . .	6
1.6	Opto-mechanical cavity (OMC) used during the internship . . . . .	7
<b>2</b>	<b>Addressing a single Optomechanical crystal</b>	<b>9</b>
2.1	Opto-mechanical interrogation . . . . .	9
2.2	Identification of optical resonances . . . . .	10
2.3	Single resonances in linear regime . . . . .	12
2.4	Opto-mechanical characterization in linear-regime . . . . .	12
2.5	Opto-mechanical characterization in non-linear regime. . . . .	13
<b>3</b>	<b>Addressing coupled Optomechanical crystals</b>	<b>18</b>
3.1	Description of the system . . . . .	18
3.2	Non-Linear and Linear resonances . . . . .	18
3.3	Two Non-Linear resonances . . . . .	21
3.4	Two Non-Linear resonances belonging to two OMCs on the same waveguide . . . . .	23
<b>4</b>	<b>Short term perspectives and preliminary results</b>	<b>27</b>
4.1	Evidence of chaotic behavior . . . . .	27
4.2	Phase control of the coupling . . . . .	27
<b>5</b>	<b>Middle term perspectives</b>	<b>28</b>
5.1	Random number generator . . . . .	28
5.2	Addressing cavity breathing modes . . . . .	30
5.3	Implement a feedback loop . . . . .	30
5.4	More than two cavities . . . . .	30
<b>A</b>	<b>Shifted resonances</b>	<b>31</b>
<b>B</b>	<b><math>Q</math> factors</b>	<b>32</b>
<b>C</b>	<b>High <math>Q</math> factor interacting resonances</b>	<b>33</b>

# 1 Introduction to opto-mechanics

Radiation pressure is a well-known physical quantity, firstly observed in the 17<sup>th</sup> century by Kepler, that describes the exchange of momentum between light and matter. It has no appreciable effects on our everyday life, since too small, but when are used nanoscale objects one can see, study and engineer its presence. In optomechanics it is the link between light and mechanical vibrations of nanostructures.

It can be visualized as a Fabry-Perot optical cavity with a movable mirror (Figure 1). The light enters the cavity and thanks to radiation pressure moves the movable mirror leading to a change in the optical resonance. So, the input laser light enters the cavity or not based on the movement of the mirror hence, by collecting the light reflections, the movement of the mirror can be measured .

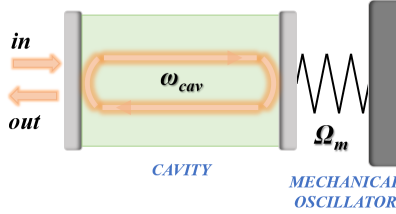


Figure 1: Optomechanical system scheme

Taking a step backward we can start considering first an optical and mechanical resonator separately, then the way in which they can interact giving rise to opto-mechanical coupling, the readout mechanism and finally a brief overview of the optomechanical devices in literature<sup>[2]</sup>.

## 1.1 Optical resonator

The easiest optical resonator that one can imagine is a one-dimensional Fabry-Perot cavity. It consists of two partially reflecting mirrors put face to face that confine light at a certain wavelength. The red box of Figure 2 shows it.

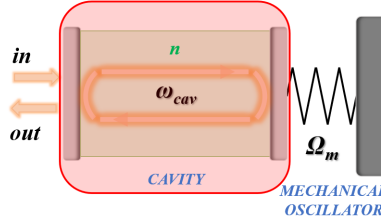


Figure 2: Fabry-Perot cavity

In it, only a finite number of radiation modes can propagate and their frequency is given by  $\omega_{cav} = m\pi \frac{c}{2nL}$  where  $m$  is an integer,  $L$  is the distance between the mirrors,  $c$  the speed of light in vacuum and  $n$  is the refractive index of the material. Considering losses of photons ( $\kappa$ ) inside the cavity that are due to not perfect mirror reflections, absorption and scattering, we can define the optical cavity quality factor ( $Q_{opt}$ ) that is a measure of the energy loss of the cavity, high  $Q$  means low losses so photons will live longer inside the cavity. It is defined as  $Q_{opt} = \omega_{cav}\tau$  with  $\tau = \kappa^{-1}$  the photon lifetime.  $\kappa$  has two contributions, one due to the losses associated to the input power that enter the cavity ( $\kappa_{ex}$ ) so, how difficult is for the light to enter the cavity and the second ( $\kappa_0$ ) includes all the internal losses, like absorption from the medium, scattering of photons outside the cavity etc. The equation that model the evolution in time of the intra-cavity field amplitude,  $\alpha(t)$ , is:

$$\dot{\alpha}(t) = -\frac{\kappa}{2}\alpha(t) + i\Delta\alpha(t) + \sqrt{\kappa_{ex}}\alpha_{in} \quad (1)$$

where  $\Delta = \omega_L - \omega_{cav}$ , is the detuning of the laser frequency with respect to the optical cavity mode frequency and  $\alpha_{in}$  is the laser input field amplitude.

We can also derive the spectral response ( $\chi_{opt}(\omega)$ , so how system behave under an external excitation at frequency  $\omega$ ) of the cavity from which can be understood the optical absorption of the cavity (link between input and in-cavity field) that will be a Lorentzian centered at the frequency of the mode sustained by the cavity.

$$\chi_{opt}(\omega) = \frac{1}{-i(\omega + \Delta) + \frac{\kappa}{2}}. \quad (2)$$

This is an approximation for cavities that have sufficiently high Q factor with respect to the free spectral range ( $\Delta\lambda_{FSR}$ ), distance between transmission peaks of the cavity, such that overlapping between resonances is avoided.

## 1.2 Mechanical resonator

Here, we focus the discussion only on the mechanical resonator of the opto-mechanical system. One can derive the elastic motion of a structure using the lumped spring, damping and mass model following Equation 3, that schematize the system in the red box of Figure 3:

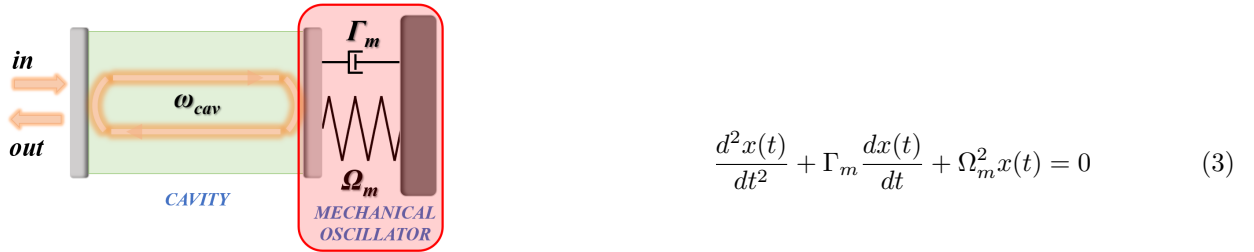


Figure 3: Lumped model

where  $\Gamma_m$  is the damping rate and  $\Omega_m = \sqrt{\frac{k}{m_{eff}}}$  is the resonance frequency, with  $k$  the spring constant,  $m_{eff}$  is the effective mass represents the real system considered that is defined as:  $m_{eff} = \rho_m \int_0^L \Phi(x)^2 dx$ , where  $\rho_m$  is the material density and  $\Phi(x)$  is the mechanical eigenmode oscillating at  $\Omega_m$ .

Solving the equation in frequency domain and introducing the mechanical susceptibility ( $\chi_m(\omega)$ , so how system behave under an external forcing at frequency  $\omega$ ) we get another Lorentzian function:

$$\chi_m(\omega) = \frac{1}{m_{eff}(\Omega_m^2 - \omega^2) - im_{eff}\Gamma_m\omega}. \quad (4)$$

The theoretically pure oscillation of the structure at  $\Omega_m$  is influenced by damping and random thermal forces (Brownian motion) that will affect its amplitude and phase giving rise to the Lorentzian shape.

Losses for mechanical systems derive from viscous medium in which the structure is immersed, the clamping of the structure that irradiate elastic waves into the substrate, anharmonic effects like phonon-phonon interactions and defects. All together contribute to the total mechanical quality factor:  $\frac{1}{Q_m} = \sum_i \frac{1}{Q_i} = \frac{\Gamma_m}{\Omega_m}$ , where  $Q_i$  are the quality factors deriving from each mechanical lossy process.

### 1.3 Opto-mechanical coupling

Considering the simplest case with one optical and one mechanical mode that are uncoupled (2 distinct oscillators), we can write that the total energy of the two systems is the sum of all energies of optical and mechanical quanta. However, in the case of a cavity with a movable mirror, the optical and mechanical oscillators must be considered as coupled oscillators to be able to consider that radiation pressure can move the mirror and change the optical cavity resonance. (System shown in Figure 1)

As suggested at the beginning, the coupling between the radiation field and the mechanical vibration is due to transfer of momentum from the photons to the matter, so radiation pressure. If a photon with given  $\lambda$  bounce on a surface and is reflected back following the same trajectory, the momentum transfer has been of  $|\Delta p| = \frac{2\hbar}{\lambda}$ . It will give rise to a radiation pressure of  $F_{RP} = \frac{2\hbar kn}{\tau_c}$  where  $n$  is the (average) number of photons that have bounced onto the surface,  $\tau_c = \frac{2L}{c}$  is the cavity round trip time.

Following this, we consider that the frequency that can sustain inside the cavity can change because of the radiation pressure that is moving the movable mirror, so:

$$\omega_{cav}(x) \approx \omega_{cav} + x\partial\omega_{cav}(x)/\partial x + \dots \quad (5)$$

where we can consider only the linear term that is said to be the optical frequency shift per displacement,  $G = \partial\omega_{cav}(x)/\partial x$ . This series expansion will allow to consider the coupling between  $\omega_{cav}$ , belonging to the optical resonator and  $x$  that is the displacement of the movable mirror.

In this situation the equations that model the evolution in time of the two oscillators, in the semi-classical (large photon and phonon numbers regime), read as:

$$\begin{cases} \dot{\alpha}(t) = -\frac{\kappa}{2}\alpha(t) + i(\Delta + Gx)\alpha(t) + \sqrt{\kappa_{ex}}\alpha_{in} \\ \ddot{x}(t) = -\Gamma_m\dot{x}(t) - \Omega_m^2x(t) + \hbar G|\alpha(t)|^2 \end{cases} \quad (6)$$

In which is easy to notice that they are coupled via  $G$  so, the evolution in time of radiation field inside the cavity depends on the elastic movements of the mirror, that is part of the optical cavity, and vice versa. They give rise to the so called optomechanical feedback loop.

### 1.4 Readout mechanism of mechanical oscillations

The optomechanical feedback loop<sup>[3]</sup> can be schematized as shown in Figure 4.

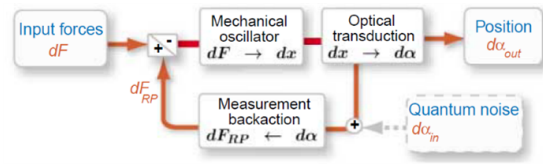


Figure 4: Optomechanical feedback loop scheme

It is describing the measurement process and its back-action on the movable mirror.

The mechanical oscillator is subject to a force  $dF$  (that can be an externally applied signal force or stress due to Brownian motion of the structure) that induces a mechanical response giving rise to displacement ( $dx$ ). The latter causes a change in the optical field (either in amplitude  $d\alpha$  or in phase, depending on the detuning  $\Delta$ ), allowing measurement of mechanical position through analysis of the output signal. For a detuned laser, the amplitude change, caused by this measurement process, feeds back to the mechanical oscillator through the radiation pressure force, closing the feedback loop. The sign of the feedback depends

on the cavity detuning and can produce either damping (red-detuned pump,  $\omega_{LASER} < \omega_{cav}$ ) or amplification (blue-detuned pump,  $\omega_{LASER} > \omega_{cav}$ ).

Considering a linear regime for the optical resonance, it is needed a high optical Q factor and a laser that is a bit detuned from the central frequency of the resonance, such that it corresponds to one of the two side-bands of the Lorentzian, to have good readout. Doing so, a small variation of the cavity length  $dx$  will be transduced in a high amplitude output signal  $d\alpha$  (Figure 5).

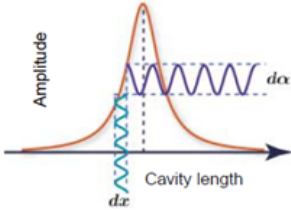


Figure 5: Mechanical oscillations transduced in optical field amplitude oscillations

### 1.5 Overview of optomechanical devices in literature

Optomechanical systems can be built with various geometries, dimensions and masses giving rise to systems suited for a very broad range of purposes, briefly resumed in the following and in Figure 6.

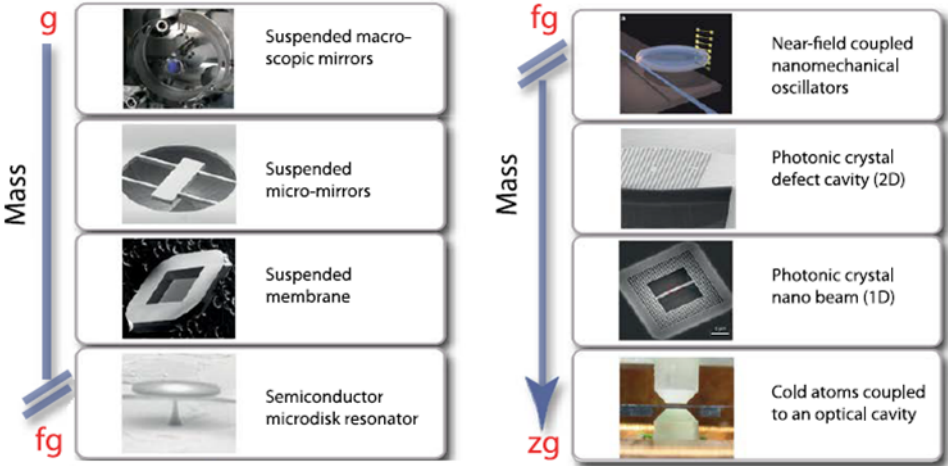


Figure 6: Optomechanical systems overview

**SUSPENDED MIRRORS:** the first way to have optomechanical interactions in a cavity is to suspend one of the cavity’s mirrors, as shown in Figure 1. The mechanical motion directly changes the cavity length and hence its frequency response. The first experimental implementations refer to the laser interferometric detection of gravitational waves.

**OPTICAL MICRO-RESONATORS:** light is guided in whispering-gallery modes along the rim of a circular resonator, like a micro-disk or micro-toroid, that exploit many different mechanical normal modes of vibration. The resulting distortions of the structure directly modify the optical path length of the resonator, shifting its optical resonance frequency and hence generating optomechanical coupling. The small size of micro-resonators allows one to generate large optomechanical coupling and access mechanical frequencies from several MHz up to some GHz.

SUSPENDED AND LEVITATED NANO-OBJECTS: here it is used a rigid optical cavity with a mechanical element either inside the cavity or in the near field of the cavity. This configuration allows an efficient optomechanical coupling to subwavelength-size mechanical objects. In essence, the mechanical motion modulates the distance  $d$  between the interfaces and since the evanescent field from the cavity decreases exponentially with  $d$ , it allows to generate optomechanical coupling.

PHOTONIC CRYSTAL CAVITIES: photonic crystals are periodic structures that can be designed to stop propagation of a given light spectrum through them. When artificial defects are introduced into the periodic pattern, localized electromagnetic field modes can form that do not decay rapidly. To obtain an optomechanical device, in-plane photonic crystal cavities are under-etched to form nanomechanical beams or membranes. Their mechanical motion results in modulations of the cavity boundaries and stresses in the material, both of which contribute to the optomechanical coupling between the cavity photons and the mechanical modes.

ULTRACOLD ATOMS: the idea of cavity optomechanics have also been implemented by using clouds of atoms. Their collective motional dynamics can resemble a single mechanical mode that, for the case of ultracold atoms, is already precooled to its quantum ground state of motion. The coupling of the collective motion of the cloud to an optical cavity field results in a position-dependent frequency shift and therefore to quantum optomechanical interactions.

### 1.6 Opto-mechanical cavity (OMC) used during the internship

The typology of optomechanical oscillator used during this internship is the one-dimensional photonic crystal beam.

The *optical resonator* is made of a photonic crystal cavity. A photonic crystal is a structure that, thanks to periodicity of the dielectric constant along one or more directions is able to allow or deny the propagation of a given spectrum of light in the directions of the periodicity creating the so-called photonic band gap (PBG). In it, photons with that energy are not able to propagate (Figure 7).

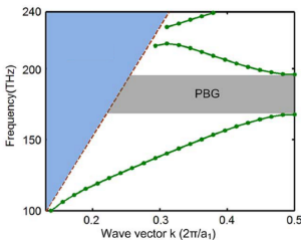


Figure 7: Photonic Band Gap around  $f = 193THz$  or  $\lambda = 1550nm$

In the simplest case (1D), it is a periodic stack of 2 different material layers. By tuning their thicknesses, dielectric constants or the number of stacks one is able to control the spectrum of light reflected and transmitted through the structure. So, it is able to act as a mirror (Bragg mirror) for a certain wavelength range. Supposing to have two of these mirrors and joining them together with a spacer in between we can create a Fabry-Perot cavity (as in Figure 2). Optical modes can sustain in it with a frequency depending on the spacer thickness and dielectric constants.

Figure 8 shows the geometry of the beam, a simulated electric field amplitude (by means of COMSOL Multiphysics) of one optical mode that can sustain in it and highlights of the cavity and mirror regions. The periodic change in the dielectric constant is accomplished by drilling holes in the structure, so the two dielectric constants will be the one of the air and the one of the beam material.

In the cavity are present holes but they have different periodicity and dimensions such that the light at  $\lambda = 1550nm$  can sustain inside the cavity with low losses.

On the two sides there are the Bragg mirrors made of rectangular holes. Their width and lattice parameters turn out to be the key feature to tune the photonic band gap in terms of bandwidth of almost zero transmission and central wavelength of the gap. The number of holes is affecting the sharpness of the gap so how large is the region needed to go from almost zero transmission to almost complete.

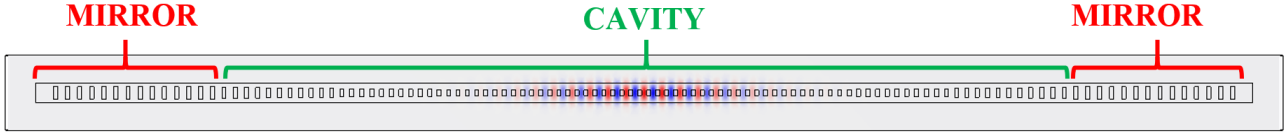


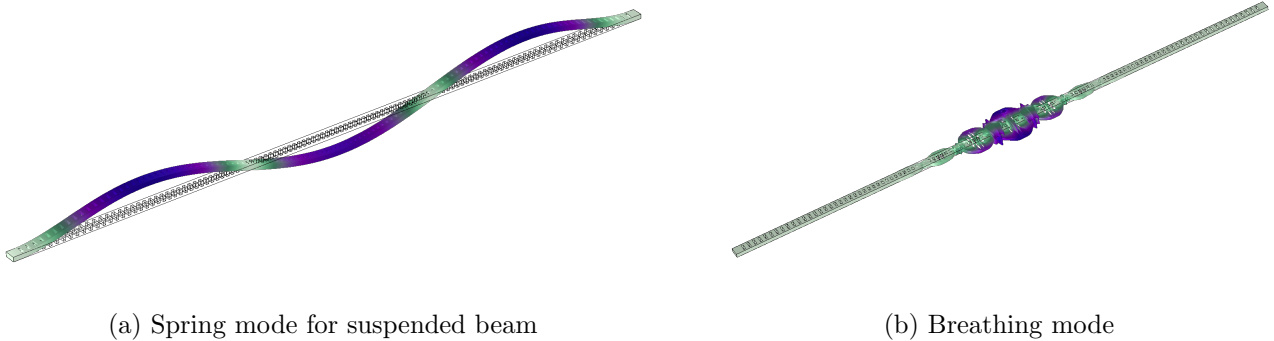
Figure 8: Optical cavity mode around  $\lambda = 1550nm$ . The color map goes from maximum positive electric field amplitude of  $2 \cdot 10^8 V/m$  (red) to the minimum one of  $-2 \cdot 10^8 V/m$  (blue). Highlights show Bragg mirrors and the cavity

The *mechanical resonator* is the beam itself that, once clamped at the two extremities, can oscillate with its own eigenmodes at their own eigenfrequencies.

There are two typologies of mechanical modes that can exist in such a structure that are the standard spring modes for suspended beam and the so called localized modes. The first ones are the most intuitive and are the eigenmodes of a standard doubly clamped beam so, there is the fundamental mode that refers to oscillation of the entire beam without any node and with zero displacement at the clamping. The second order one have one node, and following the rule, any  $n^{th}$  order mode will have  $n - 1$  nodes, both for vertical and lateral direction of oscillation, as illustrated in Figure 9a.

Instead, the localized modes are expansions and compressions of the beam transversal section localized in the cavity region, as illustrated in Figure 9b. For these modes the  $n^{th}$  order will have  $n - 1$  nodes too and because of their shape they are commonly called *breathing modes*.

Depending on the material and dimensions of the beam all those modes will sustain different frequencies. For a beam of micrometric length and nanometric thickness and width, the firsts are in the MHz range and the seconds can reach few GHz.



(a) Spring mode for suspended beam

(b) Breathing mode

Figure 9: Two typologies of mechanical modes

## 2 Addressing a single Optomechanical crystal

### 2.1 Opto-mechanical interrogation

The device used during the internship is the already discussed one-dimensional suspended photonic crystal nanobeam. The device used has been already produced before the internship start.

A model and the SEM images are shown in Figure 10a,b respectively, where can be noticed the photonic crystal nanobeams suspended on top of a waveguide designed to confine IR radiation. The model shows only one of them but, referring to the SEM image, can be noticed more suspended nanobeams on top of each waveguide.

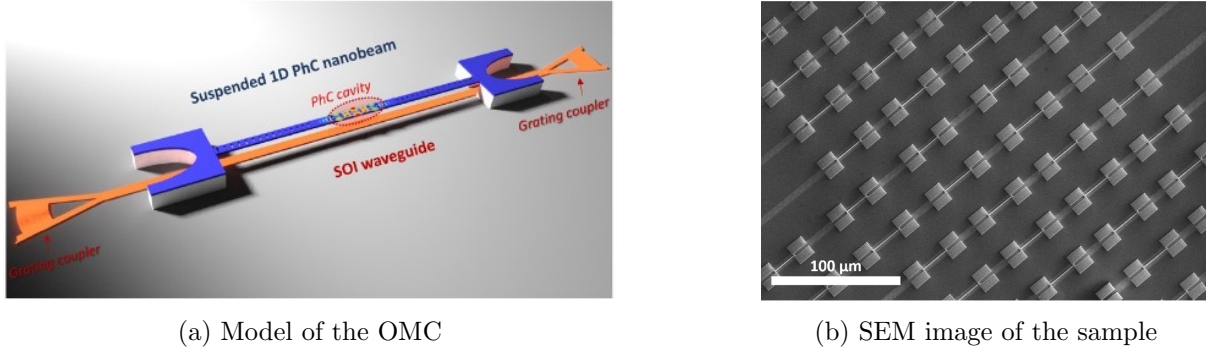


Figure 10

The subsequent lines are a summary of the device geometries and characteristics to better understand the future results.

The device is constituted by 30 waveguides in parallel, each of which is equipped with four suspended opto-mechanical cavities (OMCs) slightly different the one to each other in terms of distances between holes; more precisely the lattice constants are 325nm, 330nm, 335nm and 340nm.

The material used for the nanobeams is Indium Phosphide (InP, the blue layer in Figure 10a) and at the two extremities it is clamped to the SoI substrate via  $\text{Si}_3\text{N}_4$  supporting layer (white layer in Figure 10a). The SOI and InP/ $\text{Si}_3\text{N}_4$  parts are bonded together thanks to BCB (divinylsiloxane-benzocyclobutene) adhesive layer.

Each beam itself is made of two 10 holes Bragg mirrors designed to confine IR light around  $\lambda = 1550\text{nm}$ . In between the two mirrors there are 96 holes. The central part of cavity is made of 20 holes, and it is designed to have a photonic band gap above 193THz, that corresponds to 1550nm, such that this mode can propagate in it and other modes are suppressed. In between the central part of the cavity and the mirrors there are holes with increasing vertical dimension that are designed to reduce losses passing from the central part of the cavity to the mirror regions. The total length of a beam is around  $45\mu\text{m}$  with thickness of 300nm, width of 700nm and it is suspended onto the waveguide with a gap around 300nm.

The waveguide (in orange in Figure 10a) is made of silicon, that is suitable to confine infrared radiation around a wavelength of 1550nm, on top of  $\text{SiO}_2$  layer to limit the losses deriving from light propagation inside the *Si* substrate. Its section is  $500\text{nm} \times 200\text{nm}$ , for width and thickness respectively. Working in the infrared regime it is mono-mode so, only the fundamental mode can propagate that is the  $TE_{00}$ .

The coupling with the outworld optical fibers has been made by permanently gluing 30 fibers on top of the 30 input and output gratings.

The reading process of mechanical displacement through optical signal analysis requires light injection

through an optical fiber into the waveguide thanks to the input grating coupler. The light will propagate in it thanks to total internal reflection and because of the presence of the evanescent field that radiate from its surfaces, part of the radiation can reach the suspended structure. The evanescent field amplitude exponentially decreases but, since the gap between the waveguide and the beam is low, the light can reach it with appreciable amplitude. The coupling is enabled by the interaction between  $TE$  modes in the waveguide and in the cavity.

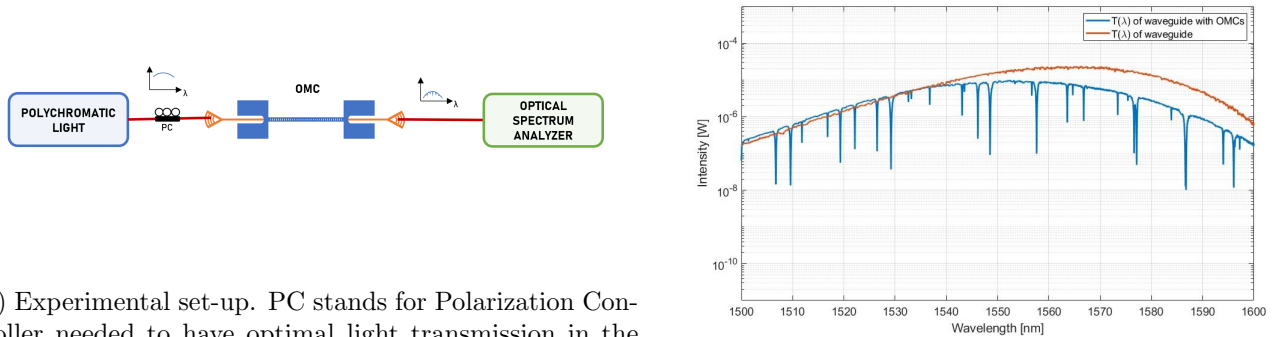
The light that enters the beam from the evanescent field remains confined in the cavity till it decays. There, it starts the optomechanical loop that is: the light enters the cavity and it can sustain if its frequency matches the cavity modes one. Due to Brownian motion of the beam, the cavity geometry is changed, and this will affect its vibrational modes changing their frequencies. It follows that, keeping fixed  $\omega_L$ , the optical cavity frequency at which the Lorentzian is centered will be red or blue detuned so the amount of light absorption inside the cavity changes (as in Figure 1). The time dependent output signal will have periods in which the light is less or more absorbed inside the cavity and it will be composed by the radiation at  $\omega_L$  modulated in amplitude by the movement of the beam that will be at lower frequencies, around MHz for spring modes and GHz for localized ones. Light in the cavity will force the cavity to undergoes strain forces because of radiation pressure.

Thinking about optomechanical coupling, since the light is confined, the localized modes will be the ones with higher coupling because of the high overlap between the optical and mechanical modes since are both limited to the cavity region.

## 2.2 Identification of optical resonances

Using a low power polychromatic source, one can analyze the light transmission through the waveguides. The setup is shown in Figure 11.a.

In the simplest case, a waveguide without any OMCs on top has been analyzed. The transmission is expected to be maximum around  $\lambda = 1550nm$  since the waveguide core and the grating coupler have been designed for that wavelength, shown as the orange curve in Figure 11.b . Adding the OMCs the general transmission spectrum is expected to be the same but with added some Lorentzian deeps corresponding to the absorption of the light inside the optical cavities (blue curve in Figure 11.b).



(a) Experimental set-up. PC stands for Polarization Controller needed to have optimal light transmission in the mono-mode waveguide.

(b) Transmission spectra with and without OMOs

Figure 11

From the acquisition of this graph, two interesting features can be extracted.

The first is to analyze to which of the four OMOs the resonances belong to and the starting point to this aim is to acquire the transmission spectrum, using polychromatic light and the OSA (Optical Spectrum Analyzer), to have a reference.

After that, by means of a tunable laser, a single resonance is excited using high power (12dBm) for ten minutes to heat up only one cavity such that some of its parameters can vary. Since the light absorption depends on the cavity parameters, so if changed under heating, every resonances of the same cavity will be shifted. Right after the heating period, the polychromatic beam is sent again, and the spectrum analyzed. By comparing the measurement before and after the heating period, one can recognize which resonances has shifted and which not and all the ones that shift will belong to the same OMC.

From the experiments the resonances result blue shifted after heating. This effect is addressed to the change of refractive index of the material after heating. By increasing the temperature, the material becomes less dense and so its refractive index  $n$  decreases.

After having performed this measurement once and having understood which resonances belong to one OMC we can proceed in the same way to identify the others. Now, fixing the laser excitation onto another resonance that in the previous case has not shift, one can be sure that modes belonging to another cavity will be addressed. This procedure can be performed three times to address the four different cavities. The first three OMCs are recognized looking at the shifts of the resonances and the fourth one by looking at the peaks that did not shift for the three previous cases.

The spectrum in Figure 12 shows a zoom after having excited the resonance at 1548.4nm. The blue curve is the reference before heating and the violet one is the measurements after heating. It can be noticed that all the other resonances did not shift. It can be noticed that also the resonance around 1558nm has shifted, telling us that they belong to the same cavity.

In Appendix A are shown more results of shifted resonances after heating.

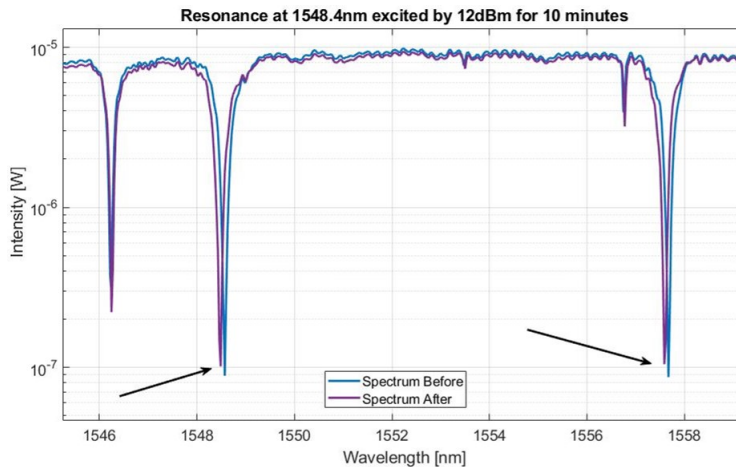


Figure 12: Shifted resonances on same OMC after heating at 12dBm for 10 minutes. The blue curve is the reference before heating and the violet one is the measurements after heating

By analyzing the shifted resonances, it can be noticed that the free spectral range,  $\Delta\lambda_{FSR}$ , between resonances belonging to the same OMC is about 10nm and this is consistent with the geometries of the Fabry-Pérot cavity. The FSR, so the distance between the top of the peaks of transmission, can be written as  $\Delta\lambda_{FSR} = \frac{\lambda_i^2}{2n_{InP}L}$  with  $n_{InP} = 3.01$  and  $\lambda_i$  that is the central frequency of the low  $\lambda$  peak considered.

By inserting  $\lambda_i = 1548.4nm$ , can be calculated  $L$  that results to be  $39.8\mu m$  that is comparable to the designed length of the cavity that is around  $35\mu m$ .

### 2.3 Single resonances in linear regime

The second is to fit with a Lorentzian function these dips to directly calculate the Q factor of the optical cavity that is a measure of how many round trips a photon will do before leaving the cavity.

To increase the measurements precision, with respect to the previous setup with polychromatic light and OSA, the resonances have excited using a tunable laser, with a wavelength step of 1pm, sending low power at -6dBm (or  $250\mu W$ ). This set-up, shown in Figure 13, will allow for a better resolution in terms of  $\Delta\lambda$  and stability in the power measurement. The output power is measured with a power meter after the photodiode transduction.

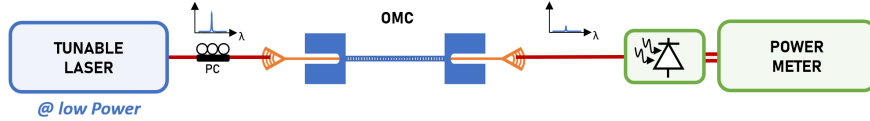


Figure 13: Set-up for optical Q factor evaluation. PC stands for Polarization Controller.

By analyzing the same waveguide as before, the output power recorded is used to retrieve the optical Q factor and understand the goodness of the optical cavity. This procedure has been done by means of Origin lab analyzing more spectral regions to show the presence of both very high- and low-quality factor optical resonances on the same waveguide with OMCs. Two representative results are shown in Figures 14.a,b.

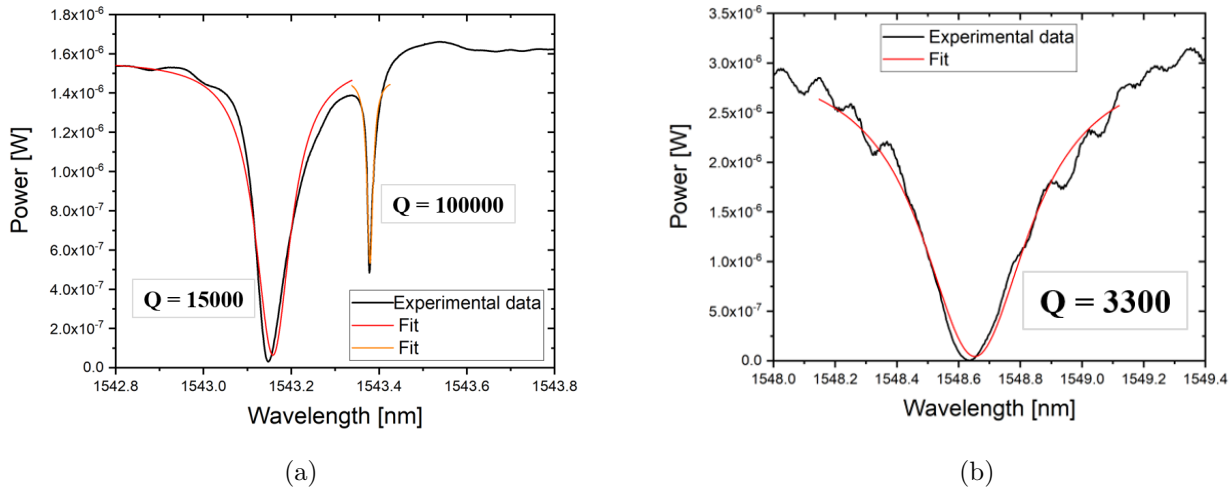


Figure 14: Optical Q factors for resonances on the same waveguide

By comparing them with previous results, about which OMCs the resonances belong to, we can say that, because of the free spectral range of around 10nm these three resonances belong to different OMCs. In Appendix B are shown more results of Q factors.

### 2.4 Opto-mechanical characterization in linear-regime

In this paragraph we focus on a single resonance analyzing the modulated optical signal going out from the waveguide both in the time and in the frequency domain, using an oscilloscope and an electric signal analyzer (ESA). In the following, by sending a low power laser beam is analyzed the resonance around  $\lambda = 1546.4nm$  (its Q factor is shown in Figure 42b, Appendix B). The experimental setup is shown in Figure 15.

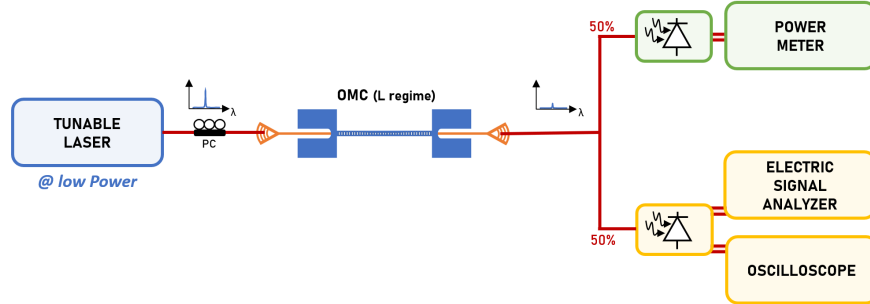


Figure 15: Set-up for optical optomechanical characterization in linear regime

The tunable laser is exciting the device and the output signal is split into two beams thanks to 50/50 fiber splitter. One part impinges on a photodiode to record the power using a power-meter and the other impinges on a InGaAs photodiode (with 3dBm attenuation at 3.5GHz) to convert the optical signal into electrical one that will be recorded in time domain by the oscilloscope and in frequency domain by the ESA.

The left images of Figures 16.a,b shows the recorded powers for forward and backward laser sweeping showing that in linear regime there is no hysteresis since the two power deeps mostly coincides (small deviation can be due to small heating during measurements). The wavy behavior of  $P(\lambda)$  is due to higher and lower transmission of the grating couplers at that specific wavelength.

In the right images, is represented a color map showing the weights (*colorbar* in dBm) of the output signal spectrum ( $x$ -axis) at a given input frequency coming from the tunable laser ( $y$ -axis) going from low to high wavelengths (represented only forward sweep because the backward one is exactly the same). It can be seen that no signal, so null spectrum, is coming out of the system for 6dBm of excitation. Whereas for 7dBm something it's happening and, around  $1546.32nm$  can be noticed a yellowish region corresponding to the steepest part of the resonance.

However, because of the low power sent, such that the optical resonances are in the linear regime, the output signal cannot be recognized from the background noise.

The horizontal lines in Figures 16.a,b refers to the laser wavelengths selected to show, in Figure 16c, the corresponding spectra. In both cases they are showing only noise, even if for 7dBm the color map shows the yellowish region around that wavelength. This region is representing a noisy output signal only with higher amplitude with respect to all the other regions.

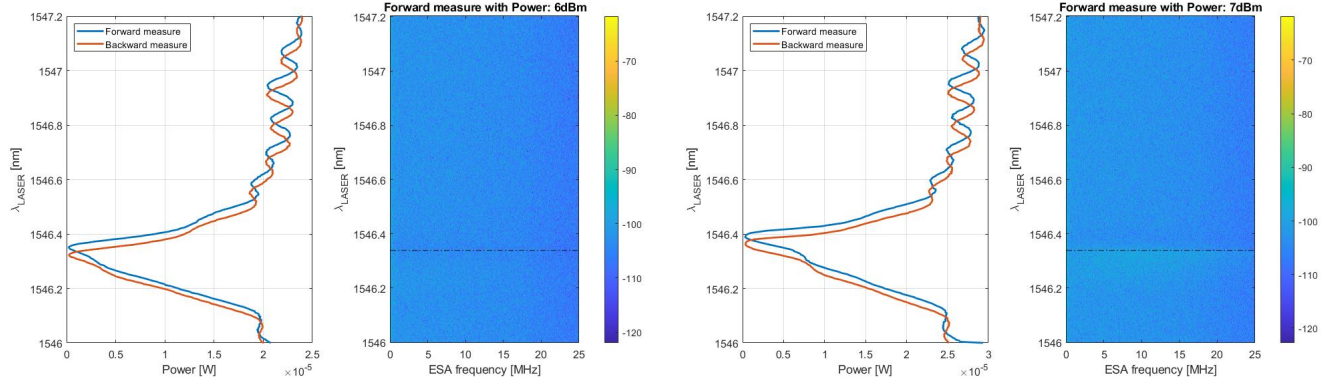
At this point it is clear that working in linear regime does not allow to see an output signal that is modulated by the elastic oscillations of the structure. The next step is to increase more the power.

## 2.5 Opto-mechanical characterization in non-linear regime.

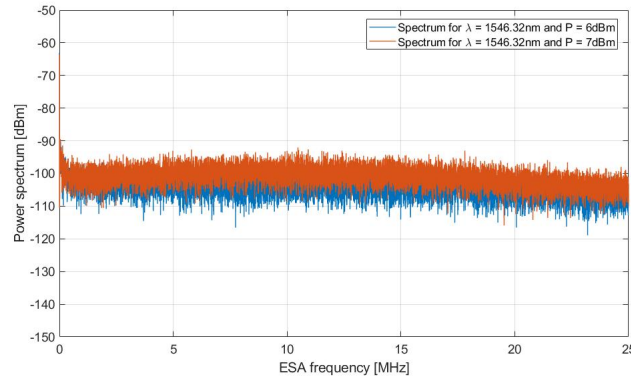
By feeding the system with higher amount of laser power, the optical resonance will enter the non-linear regime. Thanks to the heating of the system, the amplitude of Brownian motion increases, so the modulation of the optical signal due to mechanical oscillations, is expected to be visible. The setup is the same explained before (Figure 15) but the high laser power.

Before discussing the results, it is worth to give a hint of what would be expected to measure.

By increasing the power inside the optical cavity arise the thermo-optic effect where the temperature growth in the material induced by light absorption is responsible for a significant shift of the dielectric index<sup>[4]</sup>. In an optical cavity, this effect is enhanced such that it can red-shift the cavity resonance frequency. At a given input power the resonance becomes bistable. Such behavior can be evidenced by scanning forward



(a) Powers for forward and backward sweep on left and (b) Powers for forward and backward sweep on left and color map on the right for 6dBm of input laser power      color map on the right for 7dBm of input laser power



(c) Spectra at  $\lambda = 1546.32nm$  for 6dBm and 7dBm of input power showing only noise

Figure 16

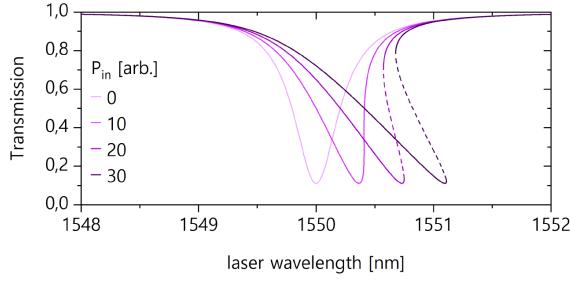
and backward the laser frequency over the resonance. By introducing the absorption rate in the cavity  $K_{abs}$  and the intra-cavity field amplitude  $\alpha$  (which evolution in time follows Equation 1), one can write that the power absorbed by the driven cavity is  $K_{abs}|\alpha|^2$ . The resulting temperature growth in the cavity related to the absorbed power through the material thermal resistance  $R_{th}$  (in units of  $KW^{-1}$ ). It leads to a temperature shift in the cavity  $\Delta\theta = R_{th}K_{abs}|\alpha|^2$ . Finally, this temperature shift induces a red-shift of the cavity resonance wavelength given by

$$\Delta\lambda = \frac{\lambda_0}{n_0} \frac{dn}{d\theta} \Delta\theta \quad (7)$$

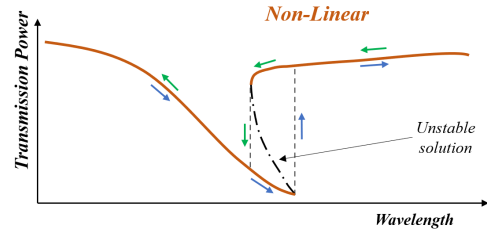
with  $\lambda_0$  and  $n_0$  respectively the resonance wavelength and the refractive index at room temperature,  $\theta = 293K$ . This will lead to an evolution of the resonance shown in Figure 17a.

In non-linear regime, by following Figure 17.b, by increasing the wavelength, following the blue arrows, the system enters the resonance and at some point it reaches the maximum absorbed power after which it abruptly jumps out of resonance in a region where the oscillation amplitude is almost null.

By decreasing the wavelength, following the green arrows, the system reaches a point for which it jumps into the resonance and so its absorbed power abruptly increases. Keeping on decreasing, the absorbed power slowly decreases and for low enough wavelength the system leaves the resonance. The wavelength values for which the system jump off or jump into the resonance are different so, the system shows hysteresis loop by sweeping the excitation wavelength.



(a) Evolution of a resonance from low to high input power



(b) Model of a non-linear resonance

Figure 17

The line-dotted part of the non-linear response refers to those points for which the solutions are not stable so the system will never pass by those points.

Going back to the experiments, in agreement with the theory, the non-linear optical resonances, for only forward sweeping of the one around  $\lambda = 1546.6nm$ , have an almost linear decrease initially till the maximum oscillation amplitude (or maximum power absorption). Then the system suddenly exits from the resonance, so the oscillation amplitude abruptly decreases (or the power absorbed abruptly decreases). The experimental output power is shown in Figure 18.

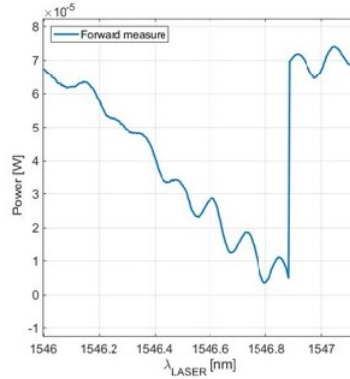


Figure 18: Experimental non-linear resonance in forward sweep. It shows  $P(\lambda_{LASER})$

Starting with an input power of 10dBm, to see if something can be measured, an output signal modulated at MHz mode can be recorded, as shown in Figure 19.

In the color map has been added three horizontal lines, respectively at  $\lambda = 1546.100nm$ ,  $1546.252nm$  and  $1546.352nm$ . For these  $\lambda$ , are shown the spectra (in the central image) and time traces (in the rightmost one) of the output signal.

In the blue case,  $\lambda = 1546.100nm$ , the system is still outside the resonance so the output signal is not modulated at any MHz frequency and both the time trace and spectrum show only noise.

In the red case,  $\lambda = 1546.252nm$ , the system entered the resonance and the time dependent output signal starts to show the typical response of abrupt deeps and then jumps back to the initial value.

In the yellow case,  $\lambda = 1546.352nm$ , the time trace shows abrupt deeps and jumps over which there will be imprinted the modulation coming from MHz mechanical modes that show the higher opto-mechanical coupling so, how much the optical cavity is deformed by the mechanical oscillations.

Regarding the shape of the time traces, a preliminary explanation is shown in Figure 20.

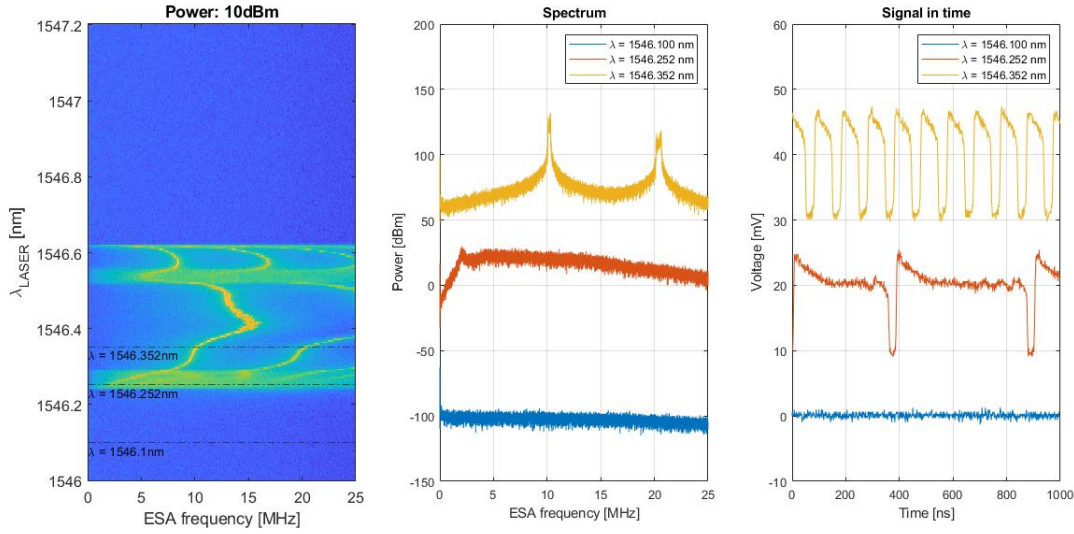


Figure 19: Color map plus spectra and time traces at the highlighted  $\lambda_{LASER}$ . Notice that in the spectrum the red signal has been shifted upward of 80dBm and the yellow one of 160dBm to better appreciate their shape. The same has been done for time signals, shifting the red one by 20mV and the yellow one by 40mV

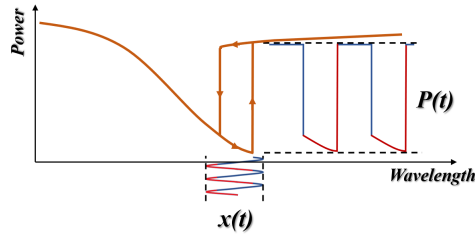


Figure 20: Interpretation of the output signal in time

The periodic modulation of the cavity  $x(t)$ , as a consequence of mechanical oscillations of the beam, will have periods for which it will determine an output signal to be high (blue part). This period will endure as long as  $x(t)$  will induce the system to reach the minimum frequency for which it can jump back into the resonance where the power is absorbed. The system will stay in the resonance as long as  $x(t)$  will induce the system to reach the maximum frequency for which it can jump out (red part).

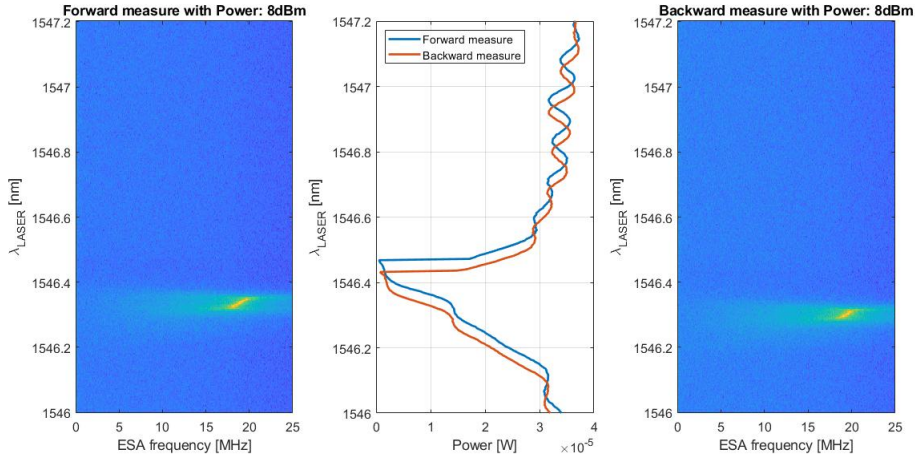
Moreover, in Figures 21.a,b, are reported two more cases similar to Figures 16.a,b, but for 8 and 10dBm of input laser power. At 8dBm it can be noticed a transition from the linear to the nonlinear regime by the appearance of the jump, the shape changes from Lorentzian to triangular (starting from 8dBm) and the appearance of the bi-stability, or hysteresis (better seen for 10dBm). The frequency difference between the value for which the system exits the resonance in forward sweeping and the one for which it enters the resonance in backward sweeping, increases more and more with the laser power increase, see Figure 21b.

Looking at the lateral graphs, so color map showing the weights (colorbar in dBm) of the output signal frequency spectrum (x-axis) at a given input frequency coming from the tunable laser (y-axis), we can see that when the amplitude of the resonance (or power absorbed) is high and very steep there is an output signal.

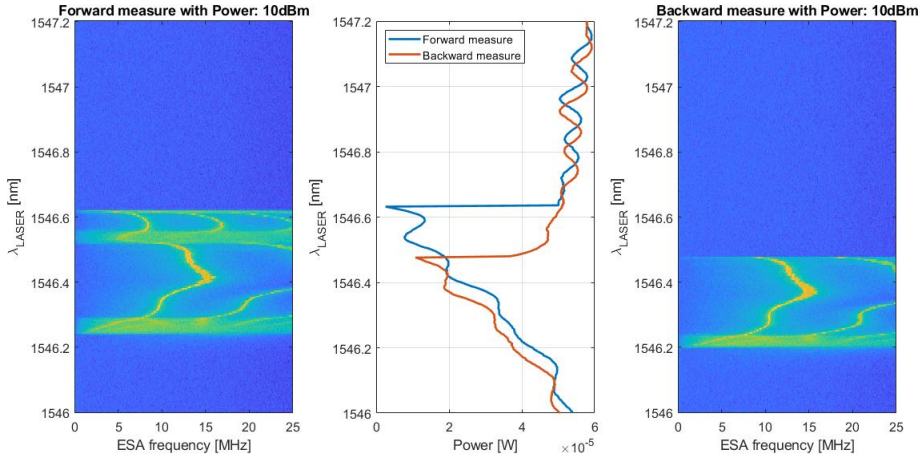
The left color maps refer to the forward sweep and the right ones to the backward. For 10dBm (Figure 21b) it is well shown that only when the system jumps into the resonance the output signal modulated by

mechanical modes can be recorded in fact, for forward measure, when the system jumps out of the resonance, around 1546.6nm, the output signal vanishes. In the backward sweep, only when the system jumps into the resonance, at 1546.5nm, the output signal can be seen again, and it will be the same as the forward one.

So, for those wavelengths we have that the mechanical displacement is efficiently transduced by the optomechanical interaction and imprinted onto the optical signal.



(a) Color maps for 8dBm in forward (left) and backward (right) laser sweep and the corresponding powers in the central image



(b) Color maps for 10dBm in forward (left) and backward (right) laser sweep and the corresponding powers in the central image

Figure 21

## 3 Addressing coupled Optomechanical crystals

### 3.1 Description of the system

In this part it will be considered the case in which two resonances interact.

Looking at the transmission spectrum through the waveguide with four OMCs (blue curve in Figure 11b), it can be easily noticed that some resonances are isolated, so around them there are no others for a quite large range, but in other cases two or more resonances are close to each other.

Since in the non-linear regime the resonance is broadened over a larger range (see Figure 21.a,b), if two resonances are close in linear regime and one or both are driven to the non-linear regime, they can overlap. So, with just one input wavelength, we can excite two different resonances belonging for sure to two different OMCs, since the free spectral range is about 10nm that is too large to have coupling between resonances of the same OMC.

We can distinguish and analyze three different ways in which we can couple two different resonances. In the following it will be shown one case for which one resonance is in non-linear regime and the other is linear and two cases for which both resonances are in non-linear regime.

### 3.2 Non-Linear and Linear resonances

To have one resonance in non-linear and one in linear regime, the setup requires to use two different waveguides with OMCs, one over which arrives high power and the other over which arrives low power. To do so there is no need to introduce attenuators since at the output of one waveguide, due to losses and absorptions, the power is quite low (around -6dBm) so it can be directly injected as input of the second waveguide.

First, it must be decided which two waveguides plus OMCs must be used. By measuring the transmission spectrum of all the 30 waveguides, using white light and OSA (setup in Figure 11a), and comparing them, one can understand which devices show two resonances close to each other. Considering spectra of waveguides with low power attenuation and that present two close resonances in the high transmission region, so between 1530nm and 1560nm, have been identified the two best for this experiment. Their spectra are shown in Figure 22 with highlighted the two resonances that have been chosen, the two around  $\lambda = 1547nm$  since they also present good Q factors (around 8000 for the first waveguide and 7100 for the second, see Appendix B). Other resonances have not been chosen because isolated, with lower Q factors or because they already presented two close resonances on the same waveguide.

In order to perform the optical coupling between the two OMCs, the setup used is described in Figure 23. It is composed by the tunable laser that excites with high power the first waveguide. The output signal (around  $\lambda = 1547nm$ ) will be modulated by the mechanical oscillations at MHz frequency that will be divided in two parts, 1% is analyzed by the first ESA and 99% is used as input of the second waveguide. The output is divided 50/50, one part goes to the power meter and the other to the second ESA and the oscilloscope, as already shown in previous setups.

For the measurements, it is worth to use the resonance of 1<sup>st</sup> waveguide in non-linear regime. This is because, as can be observed in Figure 21.a,b the high power is enlarging the resonance keeping fixed the starting point. So, high power will push the jump to happen at higher wavelengths with respect to a lower power. It is clear now that driving the resonance of the 1<sup>st</sup> waveguide in non-linear regime will allow to extend it over a region where also the resonance of the 2<sup>nd</sup> waveguide is present. The idea is schematized in Figure 24.

In the following Figure 25 is shown the results got for forward sweep. The graph on the left shows the powers measured exiting from the first resonance, in orange, and exiting the two resonances, in blue (the

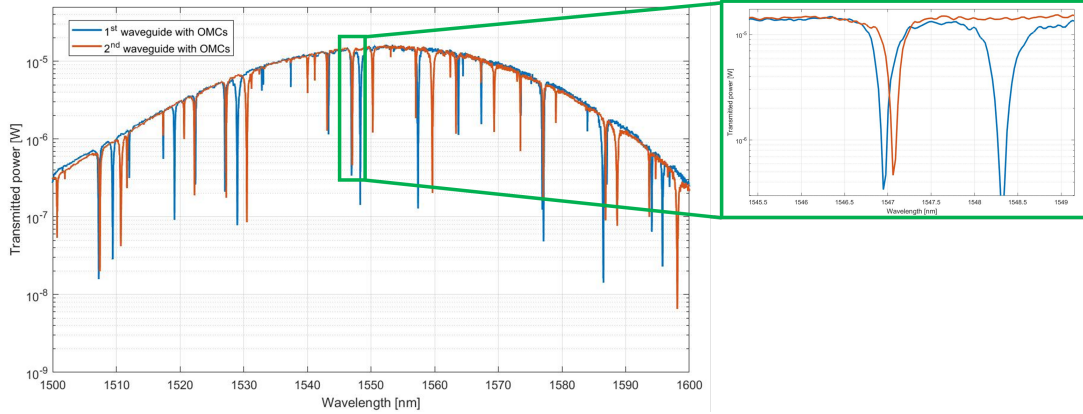


Figure 22: Transmission spectra of two waveguides with OMCs chosen and highlight on the resonances selected

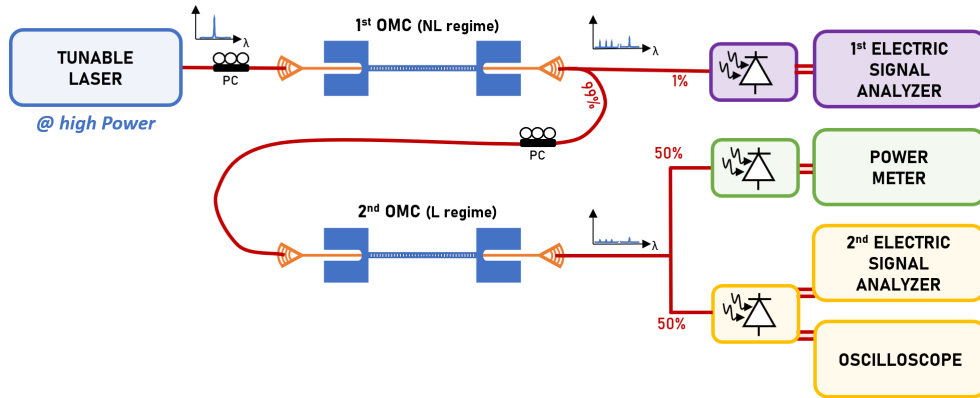


Figure 23: Set-up to excite the first resonance at high and the second at low power

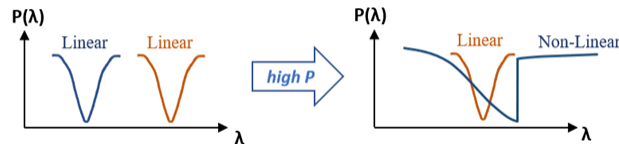


Figure 24: From two resonances in Linear regime to one in Non-Linear and one Linear regime

power exiting from the first waveguide has been measured individually).

The middle graph shows the power spectra (color map) exiting the first non-linear resonance alone.

The graph on the right shows the power spectra (color map) acquired by the second ESA so, it is analyzing the spectrum of the signal exiting the two resonances.

For these measurements, the input power of the first resonance is 11dBm and for the second is -6.5dBm.

Looking at the orange curve left graph and at the middle color map we see that they are equivalent to the ones shown in section 2.5. For the rightmost graph and blue curve, we see that both the spectrum and the power are following the previous case but for the region where there is the second resonance. By analyzing the Q factor of the linear resonance around  $\lambda = 1547.1nm$  it turns out to be around 8000 that is comparable to previous measurements taken for which the result was 7100 (see Appendix B). At  $\lambda = 1527.06nm$ , it can be noticed that the power has been totally absorbed and the spectrum shows no peaks anymore (a clearer

view of this effect is shown in Figure 26).

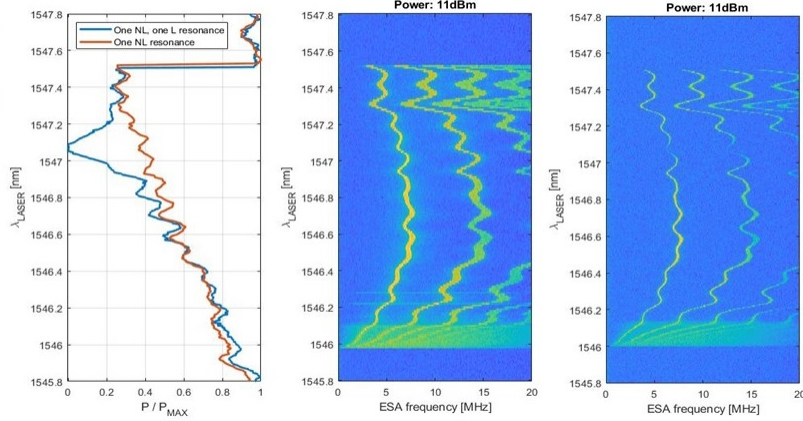


Figure 25: On the left, power behavior with isolated non-linear resonance in orange and non-linear and linear resonances in blue. Middle and right images are the color maps of isolated non-linear and non-linear and linear resonances, during forward sweep.

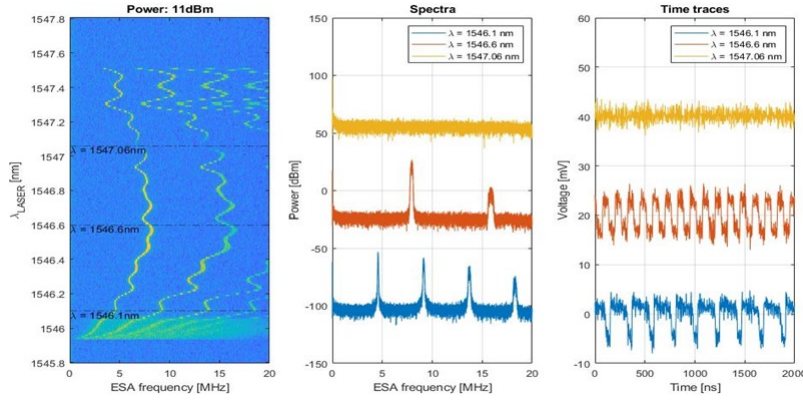


Figure 26: On the left color map of non-linear and linear resonances, during forward sweep. Middle and right, the spectra and time traces for the highlighted wavelengths

From Figure 26, referring to blue and orange time traces, they are totally equivalent to the ones coming out from a single non-linear resonance (Figure 19) so, in this case there are no appreciable consequence of the interaction. For what concerns the yellow time trace, it can be noticed that there is a complete absorption, of both the laser radiation at THz frequency and the mechanical modulation at MHz frequency, from the second linear resonance. This is in accordance to the results in section 2.4 where, if a low input power is exciting a resonance that remains in Linear regime, it is not able to transduce the mechanical oscillations into MHz modulation of the output signal.

It is worth to mention that here and in the next section, when we still talk about close resonances on different waveguides, it has been carefully checked, before and after each measurement, that all the resonances considered were isolated from other resonances on the same waveguide to avoid unwanted interactions. This step is fundamentals considering the following case of two coupled non-linear resonances on different waveguides since, if it will be skipped, we would not be able to say that the interaction is between two resonances on different waveguides, two resonances on the same waveguide or both together so, a triple interaction between two resonances on the same waveguide and one on another.

### 3.3 Two Non-Linear resonances

To have two optical resonances in non-linear regime, they must be both excited with high power. The idea is schematize in Figure 27.

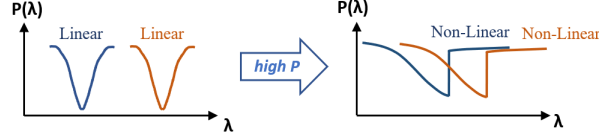


Figure 27: From two resonances in Linear regime to two in Non-Linear regime

By using the same setup of the previous section, it is not possible to achieve high powers on both. However, adding at the output of the first an optical amplifier one can amplify the output signal composed by THz radiation modulated at MHz frequency such that the input powers on both resonances are the same.

The optical spectrum amplified is quite broad with respect to the single wavelength needed to excite the two resonances and that's because the Erbium based amplifier has been designed to amplify the entire telecommunications C-band that is ranging from  $\lambda = 1530\text{nm}$  to  $\lambda = 1565\text{nm}$ . This is deleterious for the measurement that are supposed to be taken because both resonances must be excited with the same THz radiation to study their response. Figure 28 show the laser radiation at  $\lambda = 1575.3\text{nm}$ , so outside the C-band, that has been amplified and passed through the  $2^{\text{nd}}$  waveguide. We can see that in this case the laser radiation has a peak value that is almost comparable (less than one order of magnitude higher) to the amplified noise in the C-band. Here, the amplifier was amplifying 30dBm no matter the input power of the laser radiation, so in the C-band the noise was amplified by this amount.

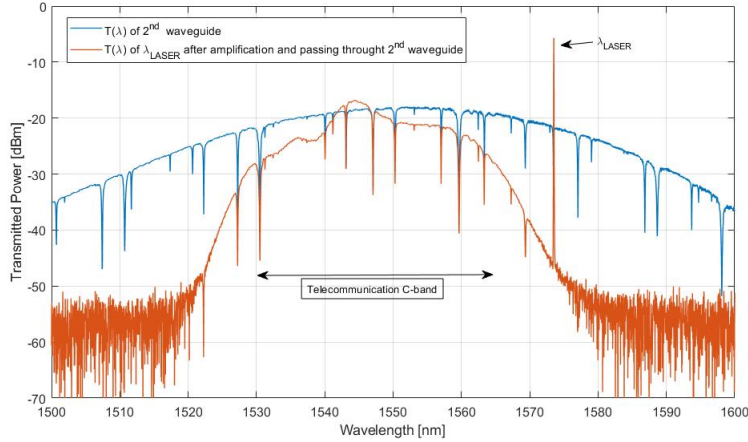


Figure 28: Spectrum amplified by the Optical Amplifier

From this graph it is clear that the measurements must be done inside the C-band such that both signal and noise are amplified by 30dBm and so the signal to noise ratio can remain almost unchanged. Moreover, to have a less noisy response coming out from the second resonance, it will be added a filter right after the amplifier that will cut the band outside the interesting region, approximately 2nm wide, that is the one for which the system enters and leave the two non-linear resonances.

The setup used is the same as the previous section with the addition of the amplifier and the filter in between the two waveguides.

The power curves in this case could not be reported since the optical power exiting from the first resonance is amplified by the amplifier to a fixed value, no matter what power enters so, after it the information on the power absorbed by the first resonance is lost. Moreover, it does not amplify to a fixed output value each wavelength, some are amplified a bit more and some others a bit less. So, having one power meter at the end of the entire setup does not allow to have a measure of the power absorbed only by the two resonances. With three power meters, one at the output of the first resonance, one at the output of the amplifier and filter and one at the end of everything will allow to measure it correctly.

In the following are shown the measurements for different input powers of the resonances around  $\lambda = 1547\text{nm}$ , as shown in the previous section. For all the measures the input powers were the same for both waveguides. In Figure 29, the left one represents the power spectra (color map) after the first resonance, from which can be clearly seen that it is exactly the one gets when an isolated optical resonance enters the non-linear regime whereas, the right image shows the power spectra (color map) after the two resonances.

In the right image, it can be seen that in a  $0.3\text{nm}$  range of wavelength, from  $1546.9\text{nm}$  to  $1547.2\text{nm}$ , the two non-linear resonances are interacting, in the following called *interaction region*. Here the two interacting oscillator are creating harmonics at frequencies that corresponds to  $\frac{1}{2}$ ,  $\frac{1}{3}$ ,  $\frac{2}{3}$ ,  $\frac{1}{4}$ , and so on, of the frequencies at which the first resonance was oscillating (the yellow curves around  $7.5\text{MHz}$  and  $15\text{MHz}$ ).

In Figure 30 are shown the power spectra (color map), three power spectra and time traces corresponding to three wavelengths in the bifurcation region. The color map is the zoom of the interaction region in the right image of Figure 29. The time traces (right image), shows the standard signal obtained till now with also a periodicity in the height of the peaks that will give rise to the peaks at fractional frequencies in the spectrum. As highlighted, if in the spectrum peaks appears at  $\frac{1}{2}$  (yellow curve) of the main peak frequency, in the time traces can be recognized a periodicity of  $2T$  on the amplitude other than the one at  $T$  of the signal outside the interaction region. If in the spectrum peaks appears at  $\frac{1}{3}$  and  $\frac{2}{3}$  of the main peak frequency, in the time traces can be recognized amplitudes periodicity of  $3T$ , and so on for higher orders bifurcations. The orange curves in Figure 30 show peaks at  $\frac{1}{5}$ ,  $\frac{2}{5}$ ,  $\frac{3}{5}$  and  $\frac{4}{5}$  so in the time traces the periodicity on the amplitude will be  $5T$ .

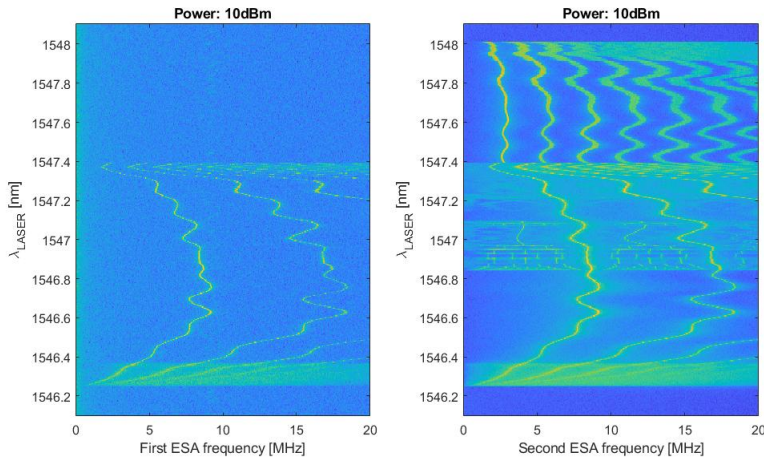


Figure 29: Color maps, on the left the one coming from the  $2^{nd}$  ESA, analyzing signal coming from 2 resonances, and on the right the one from the  $1^{st}$  ESA, analyzing signal from first resonance

From the color maps shown in Figure 29, it can be noticed that in the transitions between regions with different fractional frequencies, the output signal is very noisy showing a light green spectrum almost for any frequency. So, for those ranges of input  $\lambda$  the response of the structure tends to be more chaotic with

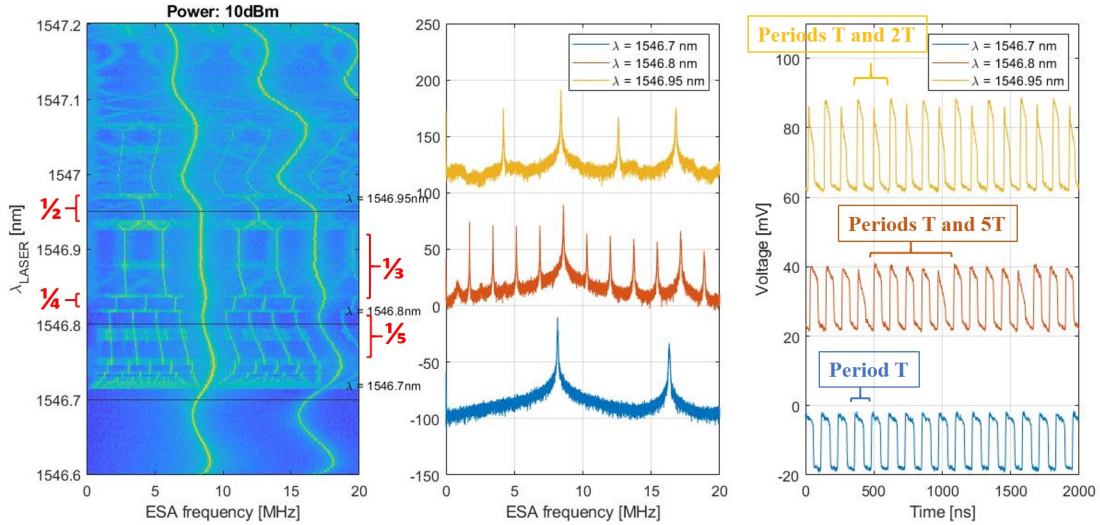


Figure 30: On the left the color maps corresponding to the zoom of the *interaction region*, in the middle and left the spectra and time traces corresponding to the highlighted wavelengths, respectively.

respect to all the other regions, see section 4.1.

This setup allow also to implement a phase control that can be addressed to study the phase change impact on the response of the two oscillators. See section 4.2.

### 3.4 Two Non-Linear resonances belonging to two OMCs on the same waveguide

The measurements shown in previous section are reported only for 10dBm because the use of the optical amplifier. It does not allow to use low powers since it has a bottom threshold for the input power to be able to amplify.

In order to overcome this limitation, one has to two non-linear resonances belonging to different OMCs but located on the same waveguide. In the following, will be shown color maps as a function of the input power to show that, by increasing it, the two resonances get closer and start to interact. Also, the interaction region will expand, in terms of laser wavelengths, as the power is increased.

In this case there cannot be any phase control since the distance between OMCs is fixed and there is no need, and no possibility, to use the amplifier since both of them belong to the same waveguide so, they will interact with the light directly injected from the laser. For these measurements the setup used is the same of Figure 15 but the high power and the fact that now the laser  $\lambda$  that will excite the system is set to sweep in a range for which there are two resonances close enough.

Looking at the transmission spectra acquired using white light (Figure 31), the waveguide chosen shows two close resonances around  $\lambda = 1543nm$ , highlighted in the zoom. In terms of wavelengths, these two resonances differ by less than 400pm so, with a powerful enough laser beam they can be coupled. The two target resonances the optical Q factors are shown in Figure 14a . The one at lower wavelength present a  $Q_{opt}$  of 15000 and the other a  $Q_{opt}$  of 100000. Since with high input power we enter the non-linear regime and extend the resonance frequency range, if the optical Q is not so high the resonance will extend more with respect to high  $Q_{opt}$  resonances. To better show this aspect, in Appendix C, are shown color maps for forward sweep at increasing powers for two close resonances with both high Q factors (around 70000). At

11dBm can be clearly seen that the interaction region is less than 100pm. So, working with the low  $Q_{opt}$  resonance at lower wavelength will allow to extend it easily to the range of wavelength for which there is the presence of the  $2^{nd}$  resonance too.

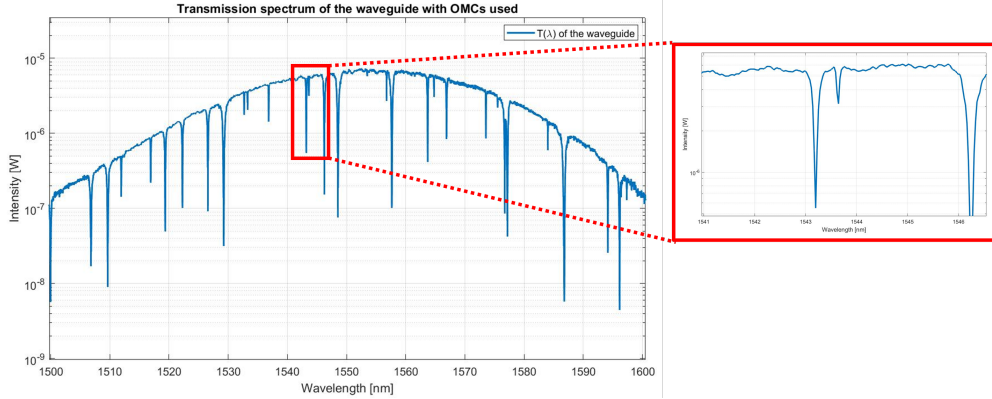


Figure 31: Transmission spectra of the waveguides with OMCs chosen and highlight on the two resonances selected

The results for only forward sweeping of the laser wavelength are shown in Figure 32 as a function of the input laser power to show that, by increasing the power, the two resonances that initially were isolated, start to expand and, in this case, for 10dBm power they start to interact showing bifurcations as in the previous section.

In this kind of setup was possible to measure the output power in the correct way since there is no intermediate amplification and the output power spectrum corresponds to the power absorbed by one or both resonances.

For these measurement it can be clearly noticed the interaction region enlarging with the increase of the power. A common way to represent it is called "Arnold Tongue"<sup>[5]</sup> that is showing, as the function of the wavelength ( $x$ -axis) and the excitation power ( $y$ -axis), how large is the interaction region. Figure 33 shows it; in yellow is the interaction region, enlarging as the power increase, and the blue region is referring to regions where no-interaction is present. The vertical line is at  $\lambda = 1543.63nm$  that is the middle wavelength of the interaction region at 9.5dBm, the one seen at the lowest power. It can be noticed that the interaction region (yellow part) is enlarging mostly for  $\lambda$  bigger than the vertical line. This is consistent with the fact that the high power is pushing the jump to happen at high wavelengths whereas the value for you enter the resonance is almost fixed.

In Figure 34 are shown on the left the power spectra (color map) acquired for the forward sweep, on the right the power spectra (color map)for backward sweep and in the middle the power curves in the two cases. In this latter graph, it can be easily seen the system leaving and jumping into the two non-linear resonances at different input wavelengths for both resonances, showing that both resonances have entered the non-linear regime.

The discrepancy between the wavelength for which the oscillator leaves and enters the non-linear resonance affect the backward measure leading to the impossibility of coupling between the two resonances. Decreasing the wavelength, the system leaves the second resonance before it can enter the first one so the two oscillators result to be uncoupled.

As shown in Figure 30, in the following Figure 35 are shown the color map, on the left, the spectra and the time traces corresponding to the three highlighted  $\lambda_{LASER}$ . For  $\lambda = 1543.62nm$  can be noticed that bifurcations lead to peaks at  $\frac{1}{11}$ ,  $\frac{2}{11}$ ,  $\frac{3}{11}$  etc. corresponding to a periodicity in the amplitude shape of the

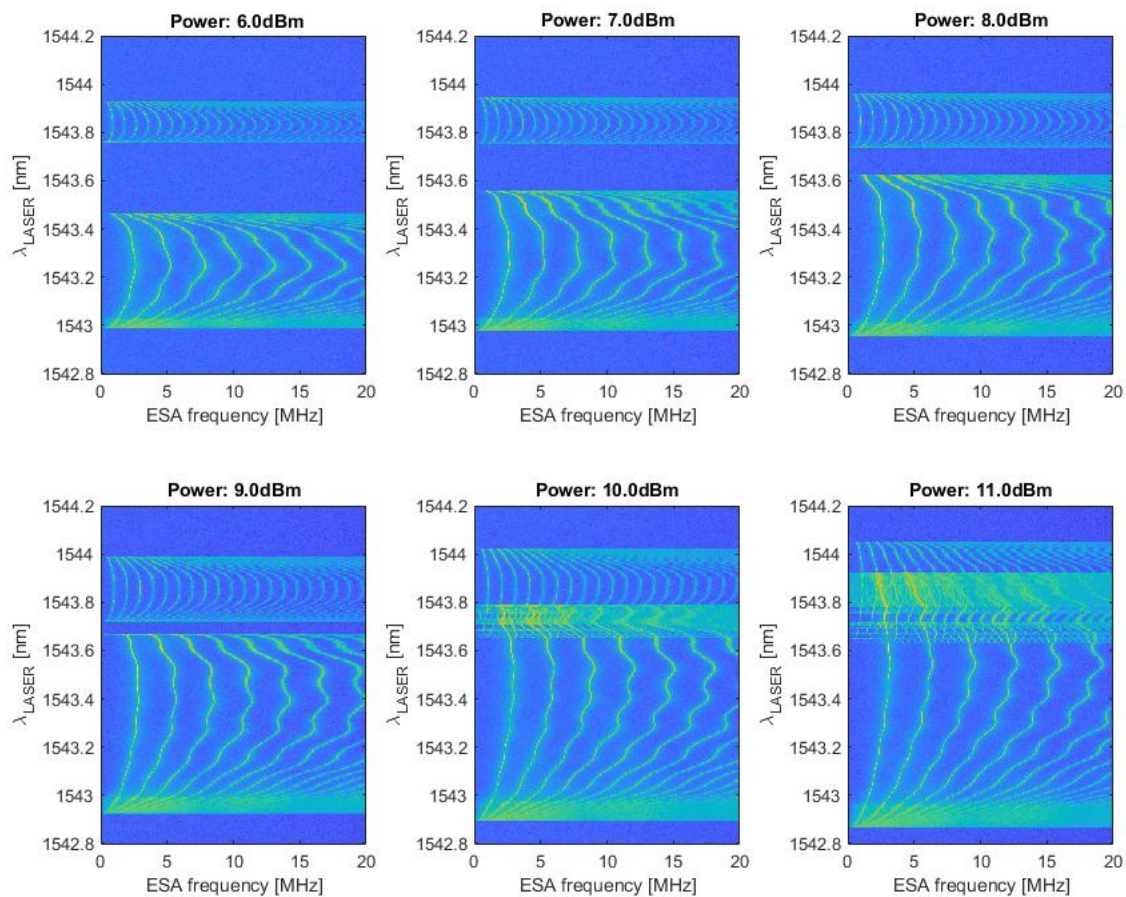


Figure 32: Color maps by increasing the input laser power show broadening of the resonances and coupling between them

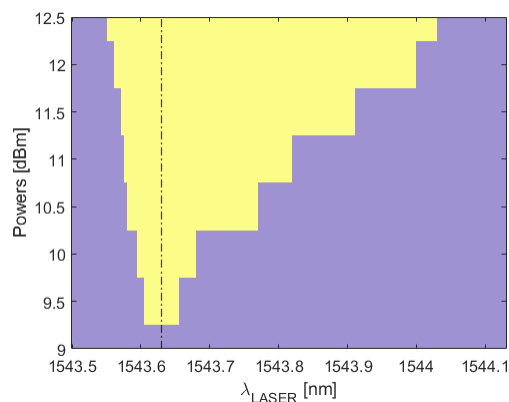


Figure 33: Arnold tongue. In yellow it is showing the width, in terms of  $\Delta\lambda$ , of the interaction region as a function of the power. In blue are depicted those regions where no interaction is present. To build this graph, more measurements, from 8dBm to 12.5dBm, were taken and are not shown in Figure 32.

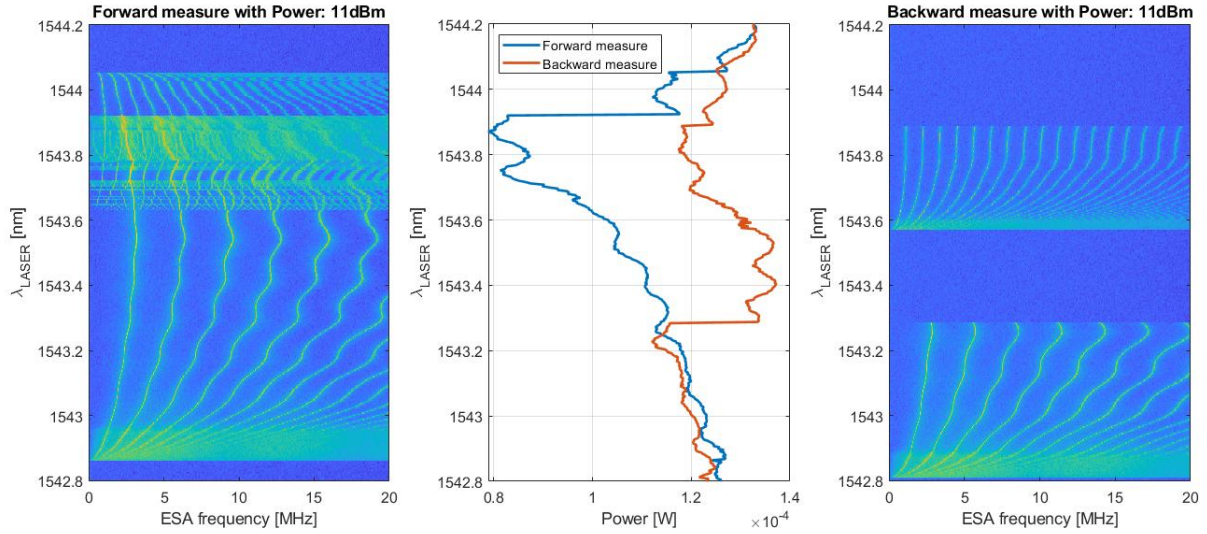


Figure 34: Color maps for forward (left) and backward (right) sweeping of the laser wavelength at 11dBm. Middle image shows powers recorded for forward (blue) and backward (orange) sweep

time traces with a periodicity of  $11T$ , where  $T$  is the period outside the interaction region. The other two wavelengths ( $\lambda = 1543.75nm$  for red and  $\lambda = 1543.85nm$  for yellow curves) are highlighting chaotic regions where the spectra do not show any clear and isolated peak. Looking at the time traces can be noticed more chaotic evolution in time with no clear periodicity.

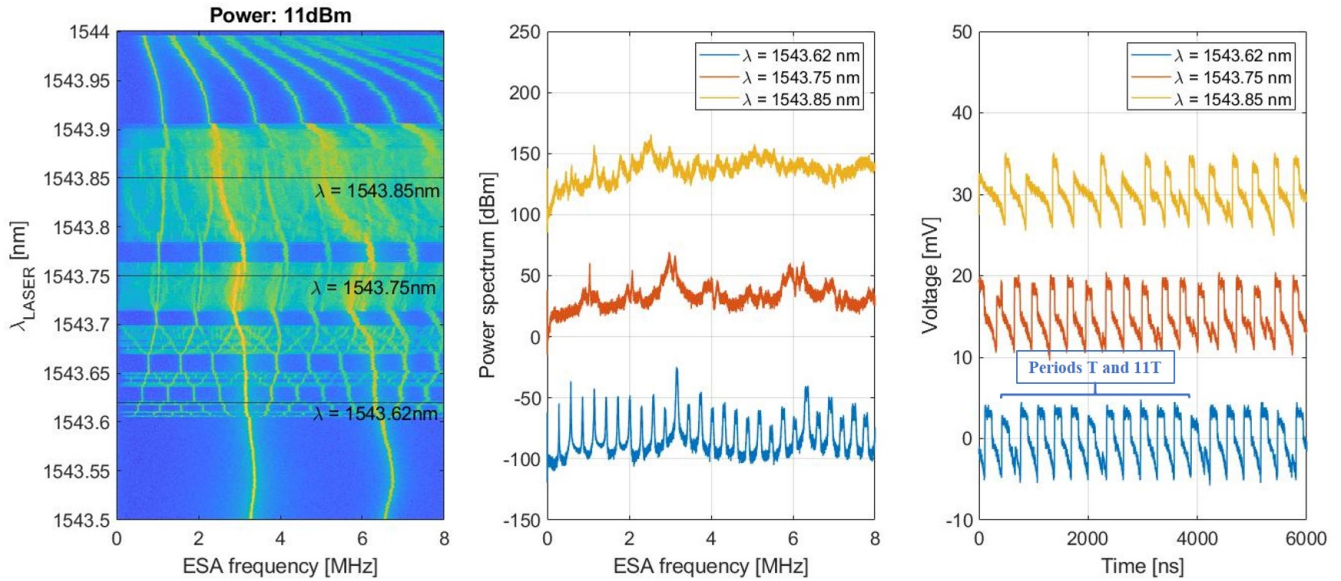


Figure 35: On the left the color maps corresponding to the zoom of the interaction region in Figure 32 for 11dBm of input power, in the middle and left the spectra and time traces corresponding to the highlighted wavelengths, respectively

## 4 Short term perspectives and preliminary results

### 4.1 Evidence of chaotic behavior

The chaotic aspect can be analyzed by means of the Lyapunov exponent<sup>[1],[6]</sup>. In mathematics, the Lyapunov exponent is a quantity that characterizes the rate of separation of infinitesimally close trajectories. Two trajectories in phase space with initial separation  $\delta\vec{Z}_0$  diverge (if it can be treated within a linear approximation) at a rate given by

$$|\delta\vec{Z}(t)| \approx e^{\lambda t} |\delta\vec{Z}_0| \quad (8)$$

where  $\lambda$  is the Lyapunov exponent.

For a system evolving in time, the maximum value that the Lyapunov exponent assumes is called the Largest Lyapunov Exponent and it is the figure of merit to refer to when the chaotic behavior of a system is studied. When it is negative the system is stable and it follows asymptotically the same trajectory in time. If it is positive the system studied is chaotic. A jump in the largest Lyapunov exponent value will be signature of the transition of the system from a regime where the oscillations are quite similar and defined in time to a more chaotic regime.

Considering the output signal time traces for a sufficient number of points such that some oscillations periods are considered. It's possible to get the Largest Lyapunov Exponent (by means of Predictive Maintenance Toolbox in Matlab) for all the time traces recorded changing the laser excitation. A preliminary result is shown in Figure 36, where can be noticed jumps to higher values of the LLE (right image) corresponding to regions in the color map (left image, corresponding to the zoom of the interaction region of Figure 32 at 11dBm) where a yellowish region is present for a large portion of MHz frequencies analyzed showing a more chaotic behavior with respect to the regions where the system is outside those regions.

Further work has to be carried out to find the correct value of the LLE and not only the behavior.

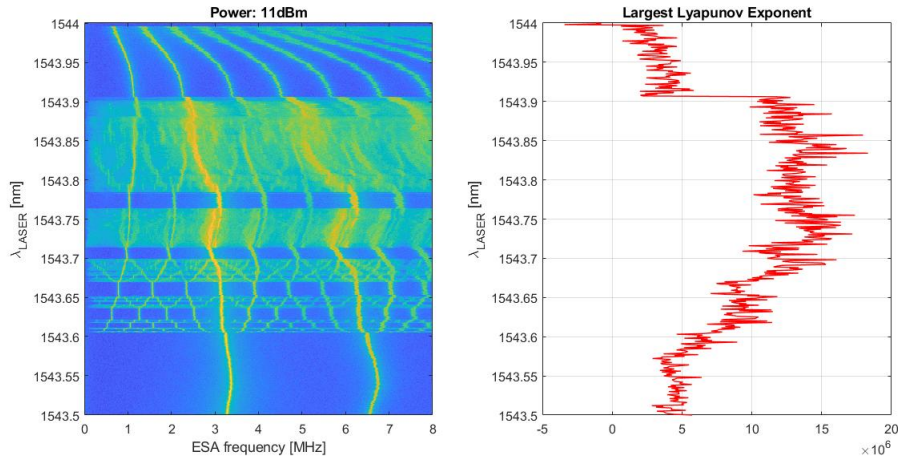


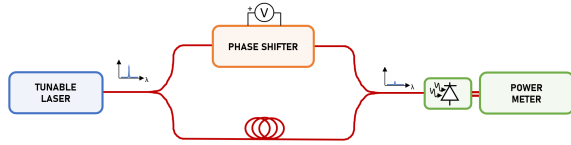
Figure 36: Color map zoomed on the interaction region on the left and LLE curve on the right

### 4.2 Phase control of the coupling

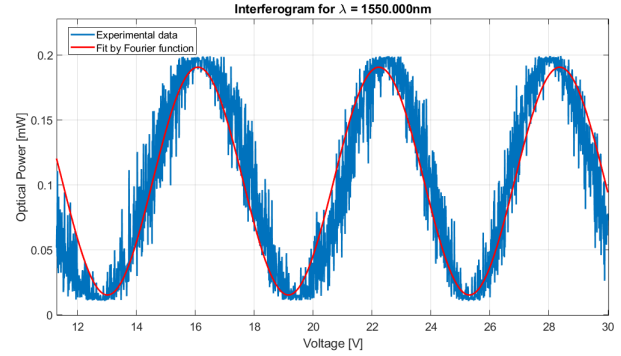
A phase shifter, that change the THz phase, can be added in between waveguides to try to act on the optical resonators' synchronization and try to understand its impact on the chaotic behavior. Doing so, maybe it can be seen some changes in the response of the system.

The phase shifter will have to be inserted in between the first and second resonance so the two non-linear resonances on two different waveguides setup must be used.

Before that, the phase shifter has been characterized building a fibered Mach-Zender interferometer (Figure 37a) with on one arm the phase shifter and on the other simple fibers to compensate for the fiber length on the phase shifter arm.



(a) Fibered Mach-Zender interferometer (MZI) for phase shifter characterization



(b) Interference pattern

Figure 37

The output signal is expected to give interference fringes as the voltage applied to the phase shifter is changed because, changing the relative phase between the beams they will create constructive or destructive interference. The output power will be maximum for constructive interference, so when the phase difference is an integer multiple of  $2\pi$  and it will be minimum for destructive interference so when the phase difference will be an odd multiple of  $\pi$ . From the characterization can be understood that are needed around 6V applied to change the THz radiation phase by  $2\pi$ . Figure 37b shows interference pattern for increasing voltage applied on the phase shifter, from 12V to 30V.

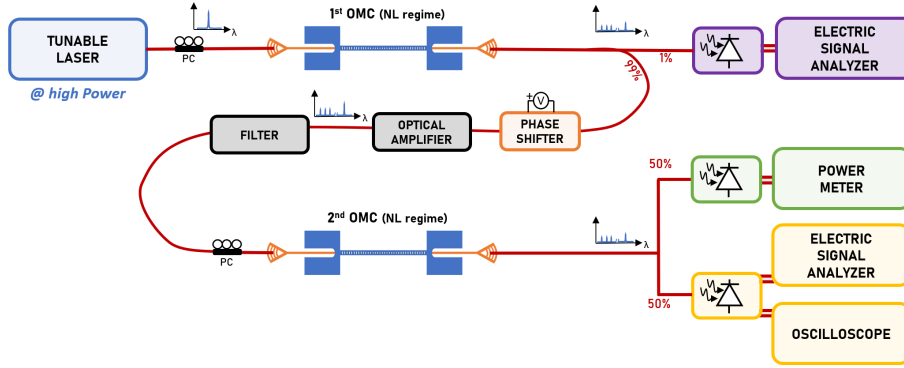
By implementing the phase shifter in the two waveguides setup, before the amplifier, (Figure 38a) it was expected to see some periodicity by sweeping the voltage applied to the phase shifter from 10V to 30V but, by fixing the laser radiation to a  $\lambda$  where the two resonances are interacting and applying the voltage to change the phase, no appreciable and reproducible results were obtained. From figure 38b can be understood that even if sometimes changes in the spectrum of the final signal (the one on the left) can be seen, they do not show any periodicity and can be compared to changes in time of the system. The image on the right shows the spectra recorded using the same laser wavelengths as before, fixed voltage on the phase shifter at 15V and without changing any other parameter, only as a function of time.

The setup is very noisy so one possibility to try to reduce the noise, would be to implement a temperature control and a better isolation with respect to the environment to be able to reduce the number of variables affecting the setup.

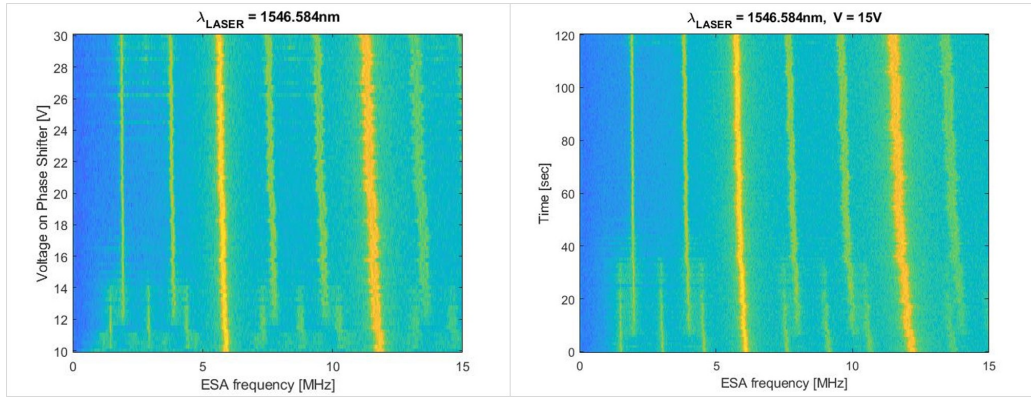
## 5 Middle term perspectives

### 5.1 Random number generator

By using two lasers at different wavelengths, two regions showing chaos can be addresses. Their output signals can be combined and used to generate random combinations of "0s" and "1s" and so, random numbers.



(a) Set-up for two waveguides with implemented the phase shifter



(b) Evolution of the spectrum with the voltage sweep (left) and in time (right)

Figure 38

A very high input power from one laser is needed to have large interaction region (Figure 39 shows it for 14dBm of input power) so to be able to put the second laser at quite different  $\lambda$ , but still inside the interaction region. Two quite different laser  $\lambda$  will allow to separate them with filters and record two distinct output signals to be combined later. The second laser will be at low power, only to "read" what is happening at a wavelength different from the high power laser one.

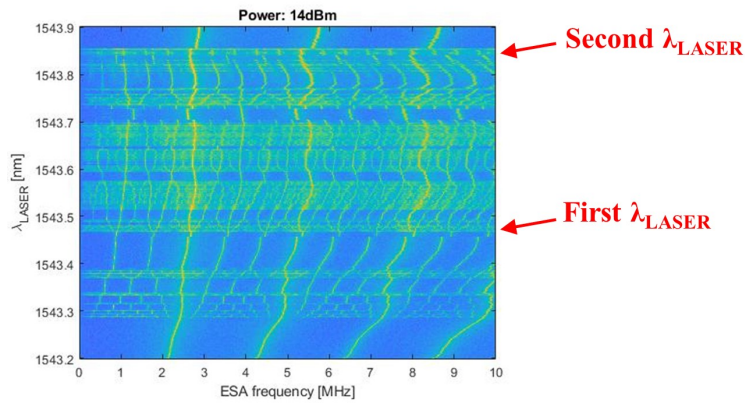


Figure 39: Color map showing the broad interaction region for an input power of 14dBm

## 5.2 Addressing cavity breathing modes

During all the discussion we have limited ourselves to MHz modulation of the output light because the GHz one, coming from the breathing modes of the cavity (Figure 9b), can not be seen.

This can be overcome by changing the material, passing from InP to GaP beams because of higher piezoelectricity of the second compound. In such devices, the presence of GHz modulation can be seen.

## 5.3 Implement a feedback loop

By implementing a feedback loop, part of the output signal can be used to feed back the system and force it to oscillate at its own frequency. Feedback loops can lead to reduction of the phase noise of the oscillation, that is a measure of how precisely an oscillator is oscillating at a fixed frequency (Figure 40).

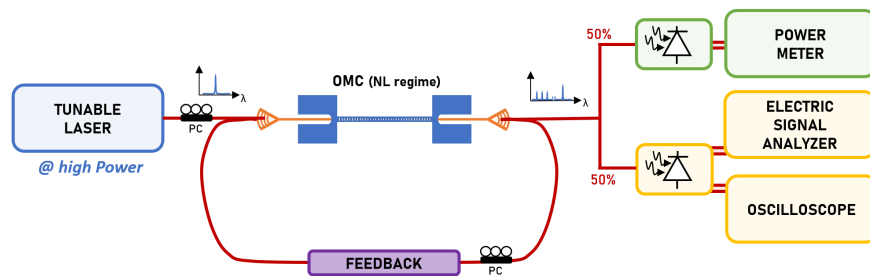


Figure 40: Scheme of feedback loop

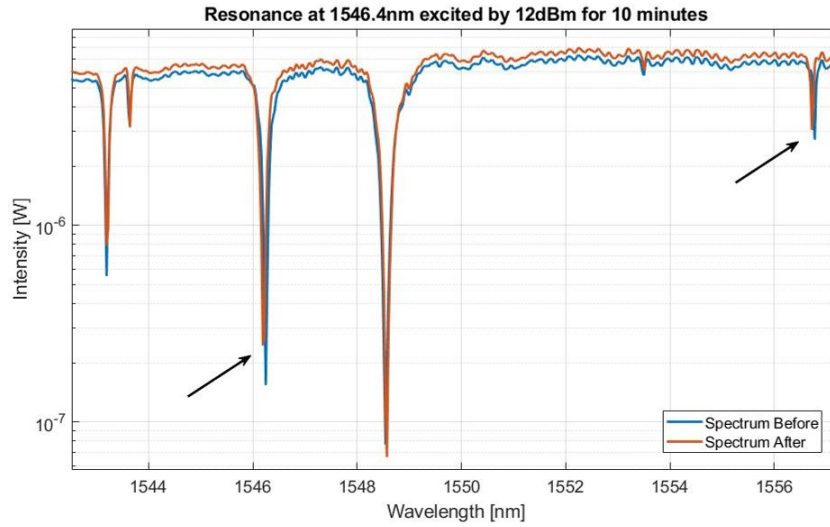
## 5.4 More than two cavities

Up to now has been used only two interacting resonances. To study more complicated dynamics there will be the need of more interacting resonances and the problem will be to find more resonances all close enough in wavelength to be excited together.

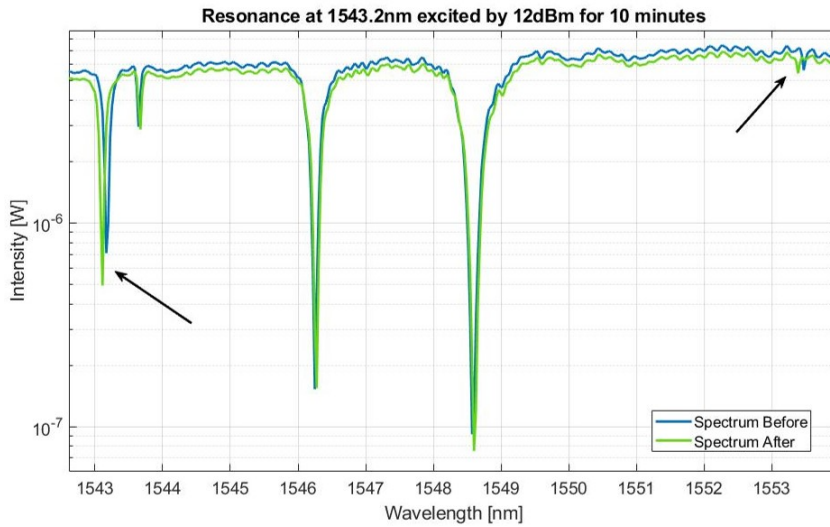
# Appendix

## A Shifted resonances

The two following Figures 41.a,b show other two measurements after the cavity heating highlighting the shifts of resonances belonging to other two OMCs. By comparing these measurements with Figure 12, and knowing that the FSR is about 10nm, can be noticed that each of the figures refer to a different OMC and since the resonance around  $\lambda = 1543.4nm$  have never shifted in the three cases, it belongs to the fourth OMC.



(a) Shifted resonances on second OMC after heating at 12dBm for 10 minutes. the blue curve is the reference before heating and the orange one is the measurements after heating



(b) Shifted resonances on third OMC after heating at 12dBm for 10 minutes. the blue curve is the reference before heating and the green one is the measurements after heating

Figure 41

## B $Q$ factors

Figures 42a,b show the  $Q$ -factors of three resonances belonging to the same waveguide of the ones in figures 14.a,b. They are showing two close-by resonances with high  $Q_{opt}$ , of about 70000 both (Figure 42.a), and an isolated resonance with  $Q_{opt}$  of about 6600 (Figure 42.b).

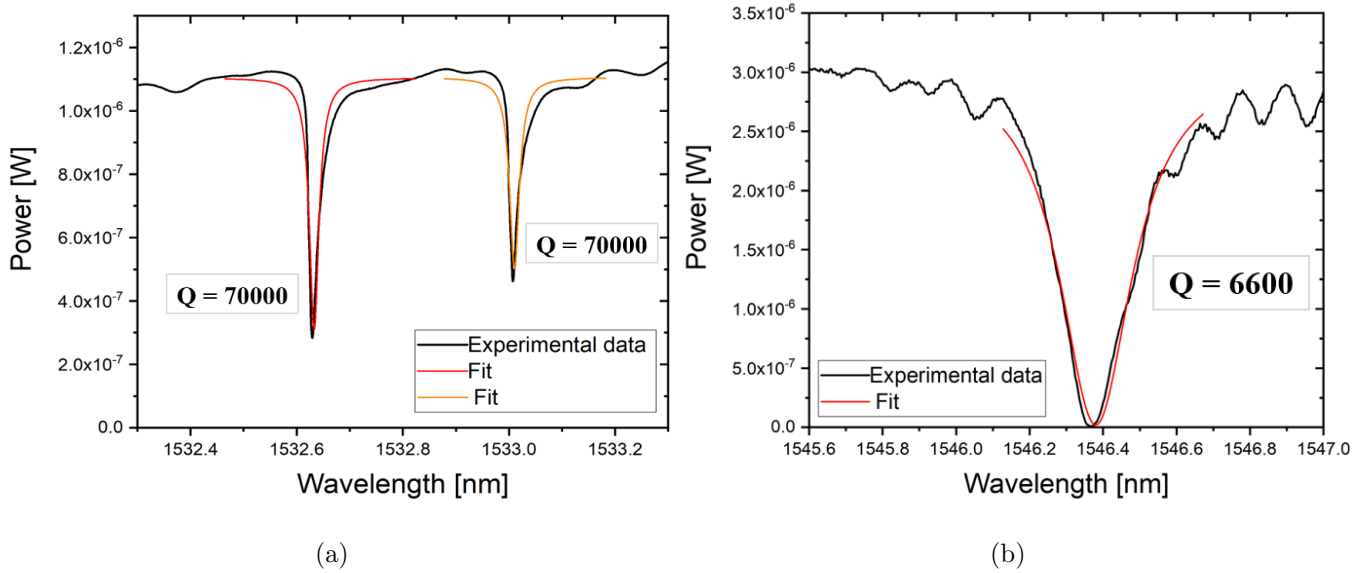


Figure 42: Optical  $Q$  factors on the same waveguide as Figures 14.a,b

Figure 43 shows  $Q_{opt}$  for the resonance on the second waveguide addressed in sections 3.2 and 3.3 with a value around 7100.

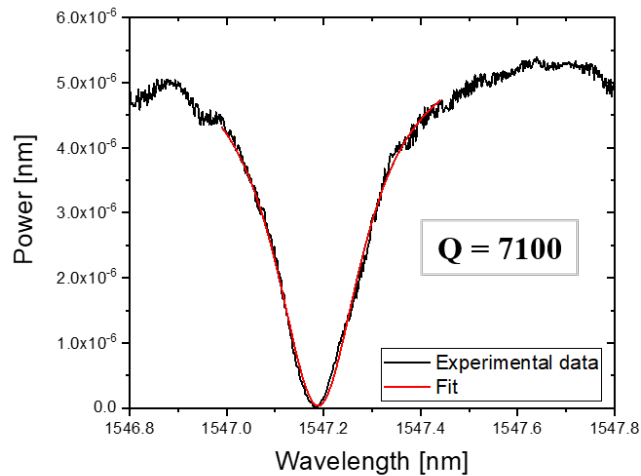


Figure 43: Optical  $Q$  factors on the second waveguide

## C High $Q$ factor interacting resonances

Figure 44 shows the color maps for increasing powers, in forward sweep of the laser wavelength, for two high  $Q$  factor resonances close enough to be coupled; more precisely are the ones with both  $Q_{opt}$  of about 70000 both in Figure 42.a. It can be noticed that for 11dBm the interaction region extends for less than 100pm in  $\lambda_{LASER}$ .

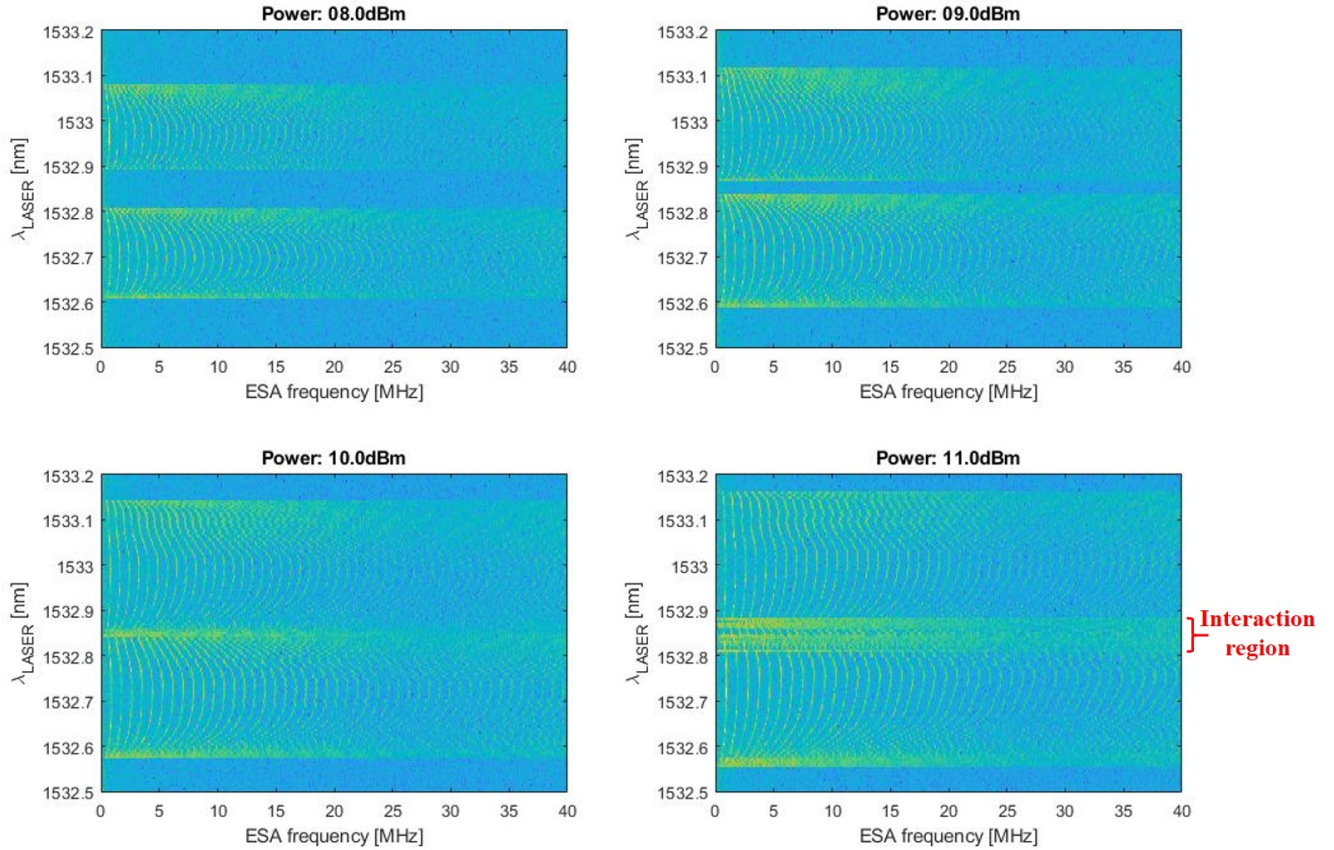


Figure 44: Color maps by increasing the input laser power show broadening of the resonances and coupling between them

## References

- [1] M. Cencini et al. “Chaos From Simple models to complex systems”. In: *World Scientific* (2010). DOI: ISBN978-981-4277-65-5..
- [2] M. Aspelmeyer T. J. Kippenberg and F. Marquardt. “Cavity optomechanics”. In: *Rev Mod Phys* 86, 1391 (2014). DOI: <https://doi.org/10.1103/RevModPhys.86.1391>.
- [3] T. J. Kippenberg and K. J. Vahala. “Cavity Optomechanics: Back-Action at the Mesoscale”. In: *Science* 321, 1172 (2008). DOI: DOI:10.1126/science.1156032.
- [4] Guilhem Madiot. “Coherent modulation in coupled electro-optomechanical photonic crystal resonators : Floquet dynamics and chaos”. In: *HAL* (2021). DOI: DOI:<https://tel.archives-ouvertes.fr/tel-03106105>.
- [5] A. Pikovsky M. Rosenblum and J. Kurths. “Synchronization: a universal concept in nonlinear sciences”. In: *Cambridge University Press, Cambridge* (2001).
- [6] R. Temam. “Infinite Dimensional Dynamical Systems in Mechanics and Physics”. In: *Cambridge: Springer-Verlag* (1988).